An analytical approach for the sequential excavation of axisymmetric lined tunnels in viscoelastic rock

H. N. Wang[*1], S. Utili[2], M. J. Jiang[3]

[1] School of Aerospace Engineering and Applied Mechanics, Tongji University, Shanghai, 200092, P.R. China

[2] School of Engineering, University of Warwick, Coventry, CV4 7AL, UK

[3] Department of Geotechnical Engineering, College of Civil Engineering, Tongji University, Shanghai, 200092, P.R. China

[*] Corresponding author

H. N. Wang,

E-mail address: wanghn@tongji.edu.cn

Tel：0086-21-65981138
Fax：0086-21-65983267

Highlights:

- An analytical solution for circular tunnels in deep rheological rock was developed
- Any number of liners and sequential excavation were accounted for
- A parametric analysis for a 3 liner support system was carried out
- Influence of excavation, liner stiffness and installation time was investigated

Abstract:

The main factors for the observed time dependency in tunnel construction are due to the sequence of excavation, the number of liners and their times of installation and the rheological properties of the host rock. In this paper, a general analytical solution accounting for all the three factors is derived for the first time.

Generalized derivation procedure for any viscoelastic models was presented accounting for the sequential excavation of a circular tunnel supported by any number of liners of different thickness and stiffness installed at different times in a viscoelastic surrounding rock under a hydrostatic stress field in plane strain axisymmetric conditions. Sequential excavation was accounted for assuming the radius of the tunnel growing from an initial value to a final one according to a time dependent function to be prescribed by the designer. The effect of tunnel advancement was also considered. For generalized Kelvin viscoelastic model, the explicit analytical closed form solutions were presented, which can be reduced to the solutions for Maxwell and Kelvin models.

An extensive parametric analysis was then performed to investigate the effect of the excavation process adopted, the rheological properties of the rock, stiffness, thickness and installation times of the liners on tunnel convergence, pressure on the liners and on the stress field in the rock for a support system made of 3 liners. Several dimensionless charts for ease of use of practitioners are provided.

Key words: sequential excavation; tunnel construction; rheological; liner; analytical solution

1. Introduction

Numerical methods such as finite element, finite difference and to a lesser extent boundary element are routinely used in tunnel design. However, full 3D analyses for an extended longitudinal section of a tunnel still require long runtime, so that the preliminary design and most of the design choices are made on the basis of simpler analytical models [1]. In fact, analytical solutions are employed as a first estimation of the design parameters also providing guidance in the conceptual stage of the design process. Parametric sensitivity analyses for a wide range of values of the input parameters of the problem are run based on them. In addition, they provide a benchmark against which the overall correctness of subsequent numerical analyses is assessed.

The main factors for the observed time dependency in tunnel construction are due to the rheological properties of the host rock [2], the sequence and speed of excavation [3, 4] and the time of installation of the liners [5]. The analytical solution derived in this paper accounts for all the three aforementioned aspects.

Concerning the first factor, most types of rocks exhibit time-dependent behavior [1], which typically continues well after the end of the excavation process. In case of sequential excavations, the observed time-dependent tunnel convergence also depends on the interaction between the prescribed steps of excavations and the natural rock rheology. After excavation, support is provided to the underground opening to reduce tunnel convergence with concrete or shotcrete liners widely employed for tunnels in rock masses. The time of installation of the liners heavily affects the observed displacements of the surrounding rock and the pressure arising between liner and rock mass which are both critical parameters for tunnel design [5]. A full analysis of the construction sequence of tunnels including the entire process of excavation and installation of the supports is paramount to obtain an engineering model to be used as a reliable design tool to determine the optimal design solutions.

In this paper, the rock rheology is accounted for by linear viscoelasticity. The so-called (according to the traditional terminology of rock mechanics [6, 7]) Kelvin, Maxwell and generalized Kelvin models will be considered. Unlike the case of linear elastic materials with constitutive equations in the form of algebraic equations, linear viscoelastic materials have their constitutive relations expressed by a set of operator equations. In general, it is very difficult to obtain analytical solutions for most of the viscoelastic problems, especially in case of time-dependent boundaries, although some closed-form or theoretical solutions have been developed for excavations in rheological rock [8, 9, 10]. However, in all these works the excavation is assumed to take place instantaneously, i.e. the process of excavation in the tunnel cross-section is ignored and only the longitudinal advancement of the tunnel face is considered, typically by introducing a fictitious lining pressure so that the problem can be mathematically cast as a fixed boundary problem. Sequential excavation is a technique becoming increasingly popular for the excavation of tunnels with large cross-section in several countries [3, 11]. For instance, 200 km of tunnels along the new Tomei and Meishin expressways in Japan, have been built via the so-called center drift advanced method. In this method, first a central pilot tunnel much smaller than the final cross-section is excavated, typically by a tunnel boring machine (TBM), then the tunnel is subsequently enlarged either by drilling and blasting or TBM to its final cross-section before the first liner is installed [11, 12]. This sequential excavation technique has been adopted by the Japanese authorities "as the standard excavation method of mountain tunnel" [13]. In several other cases of sequential excavation, the enlargement of the cross-section to its final size occurs before the installation of the first liner [3]. The analytical solution presented in this paper accounts for any time dependent excavation process employed to excavate the tunnel cross-section. Many problems of linear viscoelasticity can be solved using the principle of correspondence [14, 15, 16]. However, the cross-section of a tunnel is excavated in stages, which implies a time-dependent geometrical domain, so that the principle of correspondence cannot be employed.

Concerning the geomaterial-liner interaction, many analytical solutions have been developed for circular tunnels in elastic or visco-elastic surrounding rock [17, 18, 19, 20]. Assuming an isotropic stress state and a viscoelastic Burgers' model for the rock, Nomikos et al. [21] derived analytical solutions in closed form and performed a parametric study on the influence of the liner parameters on tunnel convergence and the mechanical response of the host rock. Different supports such as sprayed liners, two liners system and anchor-grouting support, were analyzed by Mason [22, 23, 24]. Liners were assumed to be instantaneously applied at the end of the excavation. In the tunnel practice, however, liners may be installed at any time after excavation, which is the case considered in this paper.

Supports made of two liners are very popular. However, in several recent tunnels, concrete was sprayed onto the excavation walls in steps at various times ([22, 25]) so that it becomes convenient to analyze the support system as a system made of *n* liners. Moreover, composite liners containing several rings of different materials can be analyzed conveniently as a system of several liners [23].

In this paper, an analytical formulation for the stress and displacement fields in the host rock and in the liners has been derived accounting for sequential excavation for lined circular tunnels excavated in viscoelastic rock (generalized Kelvin model with the Maxwell and Kelvin models as particular cases) and supported by any number of elastic liners installed at various times. The work presented here is applicable to a general support system made of *n* liners, therefore it is a substantial generalization of the analysis of a 2 liner support system presented in [26]. Moreover, the effect of various excavation rates, along both the radial and the longitudinal directions of the tunnel, on the response of the support system has been investigated for the first time. The tunnel face effect was considered by applying a fictitious internal pressure as in [20].

Although the obtained analytical solutions are rigorously applicable only to the axisymmetric case, i.e., a single deeply buried tunnel, Schuerch and Anagnostou [27] demonstrated that solutions achieved for axisymmetric conditions are still valid for a wide range of different ground conditions and for several cases of noncircular tunnels despite a small error being introduced.

Then a parametric study has been performed for the case of a 3 liner support in order to investigate the influence of the viscoelastic rock parameters, the excavation process, shear modulus, thickness and installation time of each liner on radial convergence and support pressure. These analyses investigate the support mechanical response for three rheological models of rock with different stiffness ratios in order to cover the wide range of responses for rock types of different viscous characteristics. Several charts of results have been plotted for the ease of use of practitioners.

2. Assumptions and definition of the problem

The excavation of a circular tunnel in rheological rock lined with a number *n* of liners set in place at various times is considered in this paper. To derive the analytical solution, the following assumptions were made:

(1) The tunnel is of circular section. The surrounding rock is homogeneous, isotropic and with its rheology suitably described by linear viscoelasticity. The tunnel is deeply buried and subject to an hydrostatic state of stress.

(2) The tunnel excavation is sequential, i.e. the tunnel radius grows from an initial value to a final one. Then liners are installed in sequence.

(3) The velocity of excavation is small enough so that no dynamic stresses are ever induced.

Regarding the simulated sequential excavation, it was assumed that the tunnel radius varies over time from an initial value R_{ini}, at time t=0, to a final radius R_{fin}, at time t=t_0. Then support is provided to the opening by installing the first liner instantaneously. The construction process can be divided into the following (n+1) stages: 1) excavation stage spanning from time $t=0$ until the time of installation of the first liner, at t=t_1, with t_1> t_0. From t=0 to t=t_0, the cross-section of the tunnel is excavated sequentially. During the time interval between t_0 and t_1, pressure is released from the rock before any support is put in place. 2) first liner stage, spanning from time t_1 to the time of installation of the second liner, t=t_2. When the first liner is put in place, at $t=t_1$, $p_1(t)$ is the contact pressure between rock and the first liner which will change in the successive stages due to the installation of the successive liners. i) i-th liner stage, spanning from time t_i to the time of installation of the i-th liner, $t=t_{i+1}$. When the i-th liner is put in place, at $t=t_i$, $p_i(t)$ is the contact pressure between the (i-1)-th liner and the i-th liner. n) n-th liner stage, spanning from time $t=t_n$ onwards (until $t=\infty$). When the n-th liner is installed, $p_n(t)$is the pressure between the (n-1)-th and the n-th liner.

At any stage, the values of the supporting pressures are different; hence we introduce a second subscript in $p_{ij}(t)$ indicating the stage of the tunneling process so that the supporting pressures between rock and liners can be written as:

$$p_1(t)=\begin{cases}0 & 0\le t<t_1\\ p_{11}(t) & t_1\le t<t_2\\ p_{12}(t) & t_2\le t<t_3\\ \vdots & \\ p_{1n}(t) & t_n\le t\end{cases},\cdots,\quad p_i(t)=\begin{cases}0 & 0\le t<t_i\\ p_{ii}(t) & t_i\le t<t_{(i+1)}\\ \vdots & \\ p_{in}(t) & t_n\le t\end{cases},\; p_n(t)=\begin{cases}0 & 0\le t<t_n\\ p_{nn}(t) & t_n\le t\end{cases}. \tag{1}$$

For this problem of axisymmetric deformation under plane strain conditions with a variable inner radius, a cylindrical coordinate system (r, θ, z) is employed. The tunnel radius $R=R(t)$ varies over time as follows:

$$R(t)=\begin{cases}R_{ini}+\psi(t) & 0\le t\le t_0\\ R_{fin} & t>t_0\end{cases} \tag{2}$$

where $\psi(t)$ is a function reflecting the actual cross-section excavation process. Note that the dependency of the tunnel radius on time makes the geometric boundary of the domain of analysis time dependent making impossible the use of analytical solutions developed in the literature for fixed boundary circular tunnels.

The effect of tunnel face advancement is very important to analyze the distribution of stresses and displacements of the concerned tunnel section [28]. But the calculation of mechanical response near the tunnel face is a three-dimensional (3D) boundary-value problem. In order to avoid the difficulty in 3D derivation, the equivalent time-dependent additional pressure is applied on internal boundary of the tunnel[20], which makes the problem reduced to a plane-strain case. In the following, this method is adopted to consider the effect of advancement. As shown in Figure 1, p_0^h is the hydrostatic in-situ stress far away from the tunnel, and $p_0 = p_0(t)$ is fictitious internal support pressure acting on the tunnel internal radius accounting for the supporting effect of the tunnel face [20]. $p_0 = p_0(t)$ progressively decreases over time from p_0^h to zero when the tunnel face is at such a distance that it has no longer effect on the considered section. A dimensionless parameter χ accounting for the tunnel face effect is introduced [20] to express the fictitious internal pressure:

$$p_0(t) = p_0^h\left[1-\chi(x)\right] \tag{3}$$

where $0 \le \chi \le 1$, and x is the distance of the section considered to the tunnel face. Since the tunnel is advancing, the distance x increases over time with $x=x(t)$ being a function of the excavation rate in the longitudinal direction. In the following analysis, sign convention is defined as positive for tension and negative for compression.

3. Mechanical analysis of rock and liners

3.1 Analysis of the rock mass

The boundary condition for the stresses in the rock mass is:

$$\sigma_r(R(t),t) = -p_1(t) - p_0(t),\quad \sigma_r(\infty,t) = -p_0{}^h. \tag{4}$$

In rock mechanics, Hooke's elastic solid and Newton's viscous liquid are used to simulate different rheological characteristics of rock masses. In general, the constitutive equations of linear viscoelastic model can be expressed in the form of convolution integrals as

$$\begin{aligned} s_{ij}(r,t) &= 2G(t) * de_{ij}(r,t), \\ \sigma_{kk}(r,t) &= 3K(t) * d\varepsilon_{kk}(r,t). \end{aligned} \tag{5}$$

where s_{ij} and e_{ij} are the deviatoric components of the stress and strain tensors σ_{ij} and ε_{ij}, respectively, i.e.,

$$\begin{aligned} s_{ij} &= \sigma_{ij} - \frac{1}{3}\delta_{ij}\sigma_{kk}\,, \\ e_{ij} &= \varepsilon_{ij} - \frac{1}{3}\delta_{ij}\varepsilon_{kk}\,, \end{aligned} \tag{6}$$

and $G(t)$ and $K(t)$ are relaxation moduli which can be expressed by material parameters of the adopted viscoelastic model. The asterisk ($*$) in Eq. (5) indicates a convolution integral the definition of which is:

$$f_1(t) * df_2(t) = f_1(t) \cdot f_2(0) + \int_0^t f_1(t-\tau)\frac{df_2(\tau)}{d\tau}d\tau. \tag{7}$$

For the case of axisymmetric deformation under plane strain conditions, the general solutions of rock mass can be derived according to the formulation reported in [29]. The radial displacement of rock mass can be written as:

$$u_r(r,t) = -\frac{1}{2r}\int_0^t [p_0{}^h - p_1(\tau) - p_0(\tau)]R^2(\tau)H(t-\tau)d\tau - \frac{3r}{2}\int_0^t p_0 I(t-\tau)d\tau \tag{8}$$

where

$$H(t) = \mathcal{L}^{-1}\left[\frac{1}{s\tilde{G}(s)}\right] \qquad I(t) = \mathcal{L}^{-1}\left[\frac{1}{s}\frac{1}{\tilde{G}(s)+3\tilde{K}(s)}\right], \tag{9}$$

with $\tilde{G}(s)$ and $\tilde{K}(s)$ being the Laplace transform of $G(t)$ and $K(t)$. Let us introduce the Laplace transform of a generic function $f(t)$ as:

$$\tilde{f}(s) = \mathcal{L}\left[f(t)\right] = \int_0^\infty \exp^{-st} f(t)dt, \tag{10}$$

and its inverse transform expressed by:

$$\mathcal{L}^{-1}[\tilde{f}(s)] = f(t) = \frac{1}{2\pi i}\lim_{\beta\to\infty}\int_{\alpha-i\beta}^{\alpha+i\beta}\tilde{f}(s)\exp^{st} dt. \tag{11}$$

The explicit expressions for the radial and hoop stresses are as follows:

$$\begin{aligned}\sigma_r &= -p_0{}^h[1-\frac{R^2(t)}{r^2}] - [p_1(t)+p_0(t)]\cdot\frac{R^2(t)}{r^2}\\ \sigma_\theta &= -p_0{}^h[1+\frac{R^2(t)}{r^2}] + [p_1(t)+p_0(t)]\cdot\frac{R^2(t)}{r^2}\end{aligned} \tag{12}$$

In case of an incompressible rock mass, that is, $K(t)\to\infty$, no displacements occur before the excavation begins, so that the second term in Eq. (8) is zero. Hence, the radial displacement is entirely due to the effect of the excavation. In order to calculate the displacements in the rock mass at any generic time $t > t_1$, all the supporting pressures acting on the liners must be determined.

3.2 Analysis of liners

In Figure 1, the radii of the cross-section involved in the calculations are shown, with R_1 being the outer radius of the first liner, R_2 the outer radius of the second liner (and also the inner radius of the first liner), … R_i being the outer radius of the *i*-th liner. Obviously liners are installed after the excavation process is complete, therefore $R_1 = R_{fin}$. According to the theory of elasticity, the radial displacements of the liners complying with the stress boundary conditions (see Figure 1) are:

$$u_{r\,1}^{L}(r,t)=-\frac{1}{2G_1^L r}\cdot\frac{R_1^{\,2}R_2^{\,2}}{R_1^2-R_2^{\,2}}[p_1(t)-p_2(t)]-\frac{1+\nu_1^L}{K_1^L}\cdot\frac{R_1^{\,2}p_1(t)-R_2^{\,2}p_2(t)}{R_1^{\,2}-R_2^{\,2}}\cdot r \quad \text{with} \quad t\geq t_1 \qquad (13)(13\text{-}1)$$

$$\vdots$$

$$u_{r\,i}^{L}(r,t)=-\frac{1}{2G_i^L r}\cdot\frac{R_i^{\,2}R_{i+1}^{\,2}}{R_i^{\,2}-R_{i+1}^{\,2}}[p_i(t)-p_{i+1}(t)]-\frac{1+\nu_i^L}{K_i^L}\cdot\frac{R_i^{\,2}p_i(t)-R_{i+1}^{\,2}p_{i+1}(t)}{R_i^{\,2}-R_{i+1}^{\,2}}\cdot r \quad \text{with} \quad t\geq t_i, \qquad (13\text{-}i)$$

$$\vdots$$

$$u_{r\,n}^{L}(r,t)=-\frac{1}{2G_n^L r}\cdot\frac{R_n^{\,2}R_{n+1}^{\,2}}{R_n^{\,2}-R_{n+1}^{\,2}}p_n(t)-\frac{1+\nu_n^L}{K_n^L}\cdot\frac{R_n^{\,2}p_n(t)}{R_n^{\,2}-R_{n+1}^{\,2}}\cdot r \quad \text{with} \quad t\geq t_n. \qquad (13\text{-}n)$$

where $G_j^L=\dfrac{E_j^L}{2(1+\nu_j^L)}$ and $K_j^L=\dfrac{E_j^L}{1-2\nu_j^L}$ $(j=1,2,\ldots,n)$ are the elastic shear and bulk moduli of the j-th liner.

4 Determination of the supporting pressures

4.1 Compatibility conditions

Since the boundary conditions on the stresses have already been imposed, the only boundary conditions on the displacement left to be satisfied concern compatibility.

(1) Imposing compatibility between the first liner and the surrounding rock leads to:

$$u_r(R_1,t)-u_r(R_1,t_1)=u_{r\,1}^{L}(R_1,t) \quad \text{with} \quad t\geq t_1 \qquad (14)$$

According to Eqs. (8) and (3), the radial incremental displacement of rock from time t_1 at a generic time $t>t_1$ is:

$$\begin{aligned}&u_r(r,t)-u_r(r,t_1)=\\&=\frac{1}{2r}\left\{\int_0^{t_1}p_0^{\,h}\chi(\tau)R^2(\tau)H(t_1-\tau)d\tau-\int_0^{t}p_0^{\,h}\chi(\tau)R^2(\tau)H(t-\tau)d\tau+R_1^{\,2}\int_{t_1}^{t}p_1(\tau)H(t-\tau)d\tau\right\}\end{aligned} \qquad (15)$$

Substituting Eqs. (13-1) and (15) into Eq. (14) yields:

$$\begin{aligned}&\frac{1}{2R_1}\left\{\int_0^{t_1}p_0^{\,h}\chi(\tau)R^2(\tau)H(t_1-\tau)d\tau-\int_0^{t}p_0^{\,h}\chi(\tau)R^2(\tau)H(t-\tau)d\tau+R_1^{\,2}\int_{t_1}^{t}p_1(\tau)H(t-\tau)d\tau\right\}\\&=-\frac{1}{2G_1^L}\cdot\frac{R_1R_2^{\,2}}{R_1^{\,2}-R_2^{\,2}}[p_1(t)-p_2(t)]-\frac{1+\nu_1^L}{K_1^L}\cdot\frac{R_1^{\,3}p_1(t)-R_1R_2^{\,2}p_2(t)}{R_1^{\,2}-R_2^{\,2}}\end{aligned} \qquad (16)$$

Simplifying:

$$\begin{aligned}&\frac{1}{2R_1}\left\{\int_0^{t_1}p_0^{\,h}\chi(\tau)R^2(\tau)H(t_1-\tau)d\tau-\int_0^{t}p_0^{\,h}\chi(\tau)R^2(\tau)H(t-\tau)d\tau+R_1^{\,2}\int_{t_1}^{t}p_1(\tau)H(t-\tau)d\tau\right\}\\&=a_{00}p_1(t)+a_{01}p_2(t)\end{aligned} \qquad (17)$$

with $a_{00}=-\frac{1}{2G_1^L}\cdot\frac{R_1R_2^{\,2}}{R_1^{\,2}-R_2^{\,2}}-\frac{1+\nu_1^L}{K_1^L}\cdot\frac{R_1^{\,3}}{R_1^{\,2}-R_2^{\,2}}$ and $a_{01}=\frac{1}{2G_1^L}\cdot\frac{R_1R_2^{\,2}}{R_1^{\,2}-R_2^{\,2}}+\frac{1+\nu_1^L}{K_1^L}\cdot\frac{R_1R_2^{\,2}}{R_1^{\,2}-R_2^{\,2}}$.

(2) Imposing compatibility between the (i-1)-th liner and the i-th liner with $2\le i<n$ leads to:

$$u_{r\,(i-1)}^L(R_i,t)-u_{r\,(i-1)}^L(R_i,t_i)=u_{r\,i}^L(R_i,t) \quad \text{with} \quad t\ge t_i \tag{18}$$

Substituting Eqs. (13-i-1) and (13-i) into the above, the following is obtained:

$$\begin{aligned}
&-\frac{1}{2G_{i-1}^L}\cdot\frac{R_{i-1}^{\,2}R_i}{R_{i-1}^{\,2}-R_i^{\,2}}[p_{i-1}(t)-p_i(t)]-\frac{1+\nu_{i-1}^L}{K_{i-1}^L}\cdot\frac{R_{i-1}^{\,2}R_ip_{i-1}(t)-R_i^{\,3}p_i(t)}{R_{i-1}^{\,2}-R_i^{\,2}}\\
&+\frac{1}{2G_{i-1}^L}\cdot\frac{R_{i-1}^{\,2}R_i}{R_{i-1}^{\,2}-R_i^{\,2}}p_{(i-1)(i-1)}(t_i)+\frac{1+\nu_{i-1}^L}{K_{i-1}^L}\cdot\frac{R_{i-1}^{\,2}R_ip_{(i-1)(i-1)}(t_i)}{R_{i-1}^{\,2}-R_i^{\,2}}\\
&=-\frac{1}{2G_i^L}\cdot\frac{R_iR_{i+1}^{\,2}}{R_i^{2}-R_{i+1}^{\,2}}[p_i(t)-p_{i+1}(t)]-\frac{1+\nu_i^L}{K_i^L}\cdot\frac{R_i^{3}p_i(t)-R_iR_{i+1}^{\,2}p_{i+1}(t)}{R_i^{2}-R_{i+1}^{\,2}}
\end{aligned} \tag{19}$$

Assuming:

$$a_{(i-1)(i-2)}=-\frac{1}{2G_{i-1}^L}\cdot\frac{R_{i-1}^{\,2}R_i}{R_{i-1}^{\,2}-R_i^{\,2}}-\frac{1+\nu_{i-1}^L}{K_{i-1}^L}\cdot\frac{R_{i-1}^{\,2}R_i}{R_{i-1}^{\,2}-R_i^{\,2}},$$

$$a_{(i-1)(i-1)}=\frac{1}{2G_{i-1}^L}\cdot\frac{R_{i-1}^{\,2}R_i}{R_{i-1}^{\,2}-R_i^{\,2}}+\frac{1+\nu_{i-1}^L}{K_{i-1}^L}\cdot\frac{R_i^{3}}{R_{i-1}^{\,2}-R_i^{\,2}}+\frac{1}{2G_i^L}\cdot\frac{R_iR_{i+1}^{\,2}}{R_i^{2}-R_{i+1}^{\,2}}+\frac{1+\nu_i^L}{K_i^L}\cdot\frac{R_i^{3}}{R_i^{2}-R_{i+1}^{\,2}}$$

$$a_{(i-1)i}=-\frac{1}{2G_i^L}\cdot\frac{R_iR_{i+1}^{\,2}}{R_i^{2}-R_{i+1}^{\,2}}-\frac{1+\nu_i^L}{K_i^L}\cdot\frac{R_iR_{i+1}^{\,2}}{R_i^{2}-R_{i+1}^{\,2}} \tag{20}$$

Eq. (19) can be expressed as:

$$a_{(i-1)(i-2)}p_{i-1}(t)+a_{(i-1)(i-1)}p_i(t)+a_{(i-1)i}p_{i+1}(t)=a_{(i-1)(i-2)}p_{(i-1)(i-1)}(t_i) \quad \text{with} \quad t\ge t_i \tag{21}$$

(3) Imposing compatibility between (n-1)-th liner and n-th liner

$$u_{r\,(n-1)}^L(R_n,t)-u_{r\,(n-1)}^L(R_n,t_n)=u_{r\,n}^L(R_n,t) \quad \text{with} \quad t\ge t_n \tag{22}$$

Substituting Eqs. (13-n-1) and (13-n) into the above, the following is obtained:

$$\begin{aligned}
&-\frac{1}{2G_{n-1}^L}\cdot\frac{R_{n-1}^{\,2}R_n}{R_{n-1}^{\,2}-R_n^{\,2}}[p_{n-1}(t)-p_n(t)]-\frac{1+\nu_{n-1}^L}{K_{n-1}^L}\cdot\frac{R_{n-1}^{\,2}R_np_{n-1}(t)-R_n^{\,3}p_n(t)}{R_{n-1}^{\,2}-R_n^{\,2}}\\
&+\frac{1}{2G_{n-1}^L}\cdot\frac{R_{n-1}^{\,2}R_n}{R_{n-1}^{\,2}-R_n^{\,2}}p_{(n-1)(n-1)}(t_n)+\frac{1+\nu_{n-1}^L}{K_{n-1}^L}\cdot\frac{R_{n-1}^{\,2}R_np_{(n-1)(n-1)}(t_n)}{R_{n-1}^{\,2}-R_n^{\,2}}\\
&=-\frac{1}{2G_n^L}\cdot\frac{R_nR_{n+1}^{\,2}}{R_n^{\,2}-R_{n+1}^{\,2}}p_n(t)-\frac{1+\nu_n^L}{K_n^L}\cdot\frac{R_n^{\,3}p_n(t)}{R_n^{\,2}-R_{n+1}^{\,2}}
\end{aligned} \tag{23}$$

Simplifying the above

$$a_{(n-1)(n-2)}p_{n-1}(t)+a_{(n-1)(n-1)}p_n(t)=a_{(n-1)(n-2)}p_{(n-1)(n-1)}(t_n) \quad \text{with} \quad t\ge t_n \tag{24}$$

where $a_{(n-1)(n-2)}$ and $a_{(n-1)(n-1)}$ is corresponding parameters in Eq. (20) when i=n.

4.2 Determination of supporting pressure in the first liner stage

In the first liner stage, only one compatibility condition (Eq. (14)) needs to be imposed, that is:

$$\frac{1}{2R_1}\left\{\int_0^{t_1} p_0{}^h\chi(\tau)R^2(\tau)H(t_1-\tau)d\tau-\int_0^{t} p_0{}^h\chi(\tau)R^2(\tau)H(t-\tau)d\tau+R_1{}^2\int_{t_1}^{t} p_{11}(\tau)H(t-\tau)d\tau\right\}=a_{00}p_{11}(t) \quad (25)$$

Eq.(25) results in a second type Volterra integral equation for $p_{11}(t)$ below:

$$p_{11}(t)=\frac{R_1}{2a_{00}}\int_{t_1}^{t} p_{11}(\tau)H(t-\tau)d\tau+\frac{R_1}{2a_{00}}\left\{\int_0^{t_1} p_0{}^h\chi(\tau)R^2(\tau)H(t_1-\tau)d\tau-\int_0^{t} p_0{}^h\chi(\tau)R^2(\tau)H(t-\tau)d\tau\right\} \quad (26)$$

The supporting pressure $p_{11}(t)$ can be calculated by solving the above equation having introduced the viscoelastic model of interest for the rock.

4.3 Determination of supporting pressures in the second liner stage

In the second liner stage, compatibility at the boundary between the first liner and rock and the first and the second liner, needs to be imposed (see Eqs. (14) and (18)). The equations are:

$$\begin{aligned}&\frac{1}{2R_1}\left\{\int_0^{t_1} p_0{}^h\chi(\tau)R^2(\tau)H(t_1-\tau)d\tau-\int_0^{t} p_0{}^h\chi(\tau)R^2(\tau)H(t-\tau)d\tau+\right.\\&\left.R_1{}^2\int_{t_1}^{t_2} p_{11}(\tau)H(t-\tau)d\tau+R_1{}^2\int_{t_2}^{t} p_{12}(\tau)H(t-\tau)d\tau\right\}=a_{00}p_{12}(t)+a_{01}p_{22}(t)\end{aligned} \quad (27)$$

$$a_{10}p_{12}(t)+a_{11}p_{22}(t)=a_{10}p_{11}(t_2) \quad \text{with} \quad t\ge t_2 \quad (28)$$

where $p_{12}(t)$ and $p_{22}(t)$ are yet unknown functions. Substituting Eq. (28) into (27) leads to achieve the integral equation for $p_{12}(t)$:

$$\begin{aligned}p_{12}(t)=&\frac{R_1a_{11}}{2(a_{00}a_{11}-a_{01}a_{10})}\int_{t_2}^{t} p_{12}(\tau)H(t-\tau)d\tau+\frac{a_{11}}{2R_1(a_{00}a_{11}-a_{01}a_{10})}\{\int_0^{t_1} p_0{}^h\chi(\tau)R^2(\tau)H(t_1-\tau)d\tau-\\&\int_0^{t} p_0{}^h\chi(\tau)R^2(\tau)H(t-\tau)d\tau+R_1{}^2\int_{t_1}^{t_2} p_{11}(\tau)H(t-\tau)d\tau\}-\frac{a_{01}a_{10}}{a_{00}a_{11}-a_{01}a_{10}}p_{11}(t_2)\end{aligned} \quad (29)$$

Hence, the supporting pressure $p_{12}(t)$ and $p_{22}(t)$ during the second liner stage can be calculated by solving Eqs. (29) and (28) in succession.

4.4 Determination of supporting pressures in the *i*-th ($i\ge 3$) liner stage

In the *i*-th liner stage, displacement compatibility conditions between first liner and rock, and between the liners, should all be satisfied. The equations are detailed as follows.

Compatibility between the first liner and the rock requires that:

$$\frac{1}{2R_1}\left\{\int_0^{t_1} p_0{}^h\chi(\tau)R^2(\tau)H(t_1-\tau)d\tau-\int_0^{t} p_0{}^h\chi(\tau)R^2(\tau)H(t-\tau)d\tau+\right.$$
$$\left.R_1{}^2\sum_{j=1}^{i-1}\int_{t_j}^{t_{j+1}} p_{1j}(\tau)H(t-\tau)d\tau+R_1{}^2\int_{t_i}^{t} p_{1i}(\tau)H(t-\tau)d\tau\right\}=a_{00}p_{1i}(t)+a_{01}p_{2i}(t) \qquad (30)(30\text{-}1)$$

whilst compatibility between a generic (k-1)-th liner and the k-th one (for $2\le k<i$) requires that:

$$a_{(k-1)(k-2)}p_{(k-1)i}(t)+a_{(k-1)(k-1)}p_{ki}(t)+a_{(k-1)k}p_{(k+1)i}(t)=a_{(k-1)(k-2)}p_{(k-1)(k-1)}(t_k) \qquad (30\text{-}2)$$

In case of k=2, compatibility between the first liner and the second one requires that:

$$a_{10}p_{1i}(t)+a_{11}p_{2i}(t)+a_{12}p_{3i}(t)=a_{10}p_{11}(t_2) \qquad (30\text{-}2\text{bis})$$

Finally, compatibility between the (i-1)-th liner and the i-th one requires that:

$$a_{(i-1)(i-2)}p_{(i-1)i}(t)+a_{(i-1)(i-1)}p_{ii}(t)=a_{(i-1)(i-2)}p_{(i-1)(i-1)}(t_i) \qquad (30\text{-}i)$$

The supporting pressures up to the (i-1)-th stage, $p_{1j}(t)$, $p_{2j}(t)$, $p_{3j}(t)$, $\cdots$ and $p_{ij}(t)$ with $j=1,2,\cdots,i-1$ are known from the calculations relative to the previous (i-1)-th liner stages. Hence, in the system of i equations written above (Eq. (30)), there are i unknown functions expressing the supporting pressures to be determined: $p_{1i}(t)$, $p_{2i}(t)$, $p_{3i}(t)$, $\cdots$, $p_{ii}(t)$. It is also straightforward to see that the equations are coupled.

Apart from Eq. (30-1), all the other equations, from Eq. (30-2) to Eq. (30-i), are linear in the unknowns p_{2i}, p_{3i}, $\cdots$, p_{ii}; so it is convenient to write them in matricial form to work out the solution of the system of i-1 equations (from Eq. (30-2) to (30-i). Defining:

$$\boldsymbol{A}=\begin{bmatrix} a_{11} & a_{12} & & & & \\ a_{21} & a_{22} & a_{23} & & 0 & \\ & & \ddots & & & \\ & & 0 & & & \\ & 0 & & a_{(i-2)(i-3)} & a_{(i-2)(i-2)} & a_{(i-2)(i-1)} \\ & & & & a_{(i-1)(i-2)} & a_{(i-1)(i-1)} \end{bmatrix}_{(i-1)\times(i-1)},\ \boldsymbol{B}=\begin{bmatrix} a_{10} & & & & \\ & a_{21} & & 0 & \\ & & a_{32} & & \\ & 0 & & 0 & \\ & & & & a_{(i-1)(i-2)} \end{bmatrix}_{(i-1)\times(i-1)},$$

with $\boldsymbol{A}$ and $\boldsymbol{B}$ square matrices of i-1 size; and

$$\boldsymbol{m}=\left[p_{2i}(t),\quad p_{3i}(t),\quad \cdots\quad p_{ii}(t)\right]_{1\times(i-1)}^T,\ \boldsymbol{q}=\left[p_{1i}(t),\quad 0,\quad \cdots\quad 0\right]_{1\times(i-1)}^T,$$

$$\boldsymbol{w}=\left[p_{11}(t_2),\quad p_{22}(t_3),\quad \cdots\quad p_{(i-1)(i-1)}(t_i)\right]_{1\times(i-1)}^T$$

with $\boldsymbol{m}$, $\boldsymbol{q}$, $\boldsymbol{w}$ vectors of i-1 length, Equations (30-2) to (30-i) can be written in matrix form as follows:

$$\boldsymbol{Am}=-a_{10}\boldsymbol{q}+\boldsymbol{Bw} \qquad (31)$$

and solved for $\boldsymbol{q}$:

$$\boldsymbol{m} = -a_{10}\boldsymbol{A}^{-1}\boldsymbol{q} + \boldsymbol{A}^{-1}\boldsymbol{B}\boldsymbol{w} \tag{32}$$

Hence, the integral equation for $p_{1i}(t)$ can be established by substituting the analytical expression for $p_{2i}(t)$ obtained from Eq. (32) into Eq. (30-1). Then, solving the integral equation and substituting $p_{1i}(t)$ into Eq. (32), all the other unknown supporting pressures are determined. In the particular case of 3 liners, i=3, Eq. (31) becomes the following linear system:

$$\begin{bmatrix} a_{11} & a_{12} \\ a_{21} & a_{22} \end{bmatrix}\begin{bmatrix} p_{23}(t) \\ p_{33}(t) \end{bmatrix} = -a_{10}\begin{bmatrix} p_{13}(t) \\ 0 \end{bmatrix} + \begin{bmatrix} a_{10} & 0 \\ 0 & a_{21} \end{bmatrix}\begin{bmatrix} p_{11}(t_2) \\ p_{22}(t_3) \end{bmatrix},$$

which is straightforward to verify that corresponds to Eq. (30-2bis) and Eq. (30-i) together with i=3. In section 6 of the paper, the case of 3 liners will be employed to run a parametric study to investigate the influence of the material (rock and liners) parameters, excavation rate, liners installation time, shear modulus and thickness on the tunnel radial convergence and the stress and strain fields in the host rock and the liners.

5 Solutions for the generalized Kelvin viscoelastic model

Rock masses of good mechanical properties or subject to low stresses exhibit limited viscosity. For this type of behavior, the generalized Kelvin viscoelastic model (see Figure 2a) is commonly employed [24]. Instead, weak, soft or highly jointed rock masses and/or rock masses subject to high stresses are prone to excavation induced continuous viscous flows. In this case, the Maxwell model (see Figure 2b) is suitable to simulate their rheology since it is able to account for an instantaneous elastic response followed by a long term viscous response. Here, the analytical solution will be developed for the generalized Kelvin model. The constitutive parameters of this model are: the elastic shear moduli G_H, due to the Hookean element in the model, and G_K, due to the spring element of the Kelvin component, and the viscosity coefficient η_K due to the dashpot element of the Kelvin component (see Figure 2). The solution for the Maxwell model can be obtained as a particular case of the generalized Kelvin model, for G_K=0. Note that also the solution for the Kelvin model (see Figure 2c) can be obtained as another particular case of the generalized Kelvin model, for $G_H \to \infty$.

Assuming that the rock is incompressible, the two relaxation moduli appearing in the constitutive equations (see Eq. (5)) are as follows:

$$G(t)=\frac{{G_H}^2}{G_H+G_K}\exp^{-\frac{G_H+G_K}{\eta_K}t}+\frac{G_K\cdot G_H}{G_H+G_K},\quad K(t)=\infty. \tag{33}$$

Substituting Eq. (33) into Eq. (9) yields:

$$H(t)=\frac{1}{G_H}\delta(t)+\frac{1}{\eta_K}\exp^{-\frac{G_K}{\eta_K}t},\quad I(t)=0 \tag{34}$$

Then substituting Eq. (34) into Eq. (8), the radial displacement of rock becomes:

$$u_r\left(r,t\right)=-\frac{1}{2r}\left\{\frac{1}{G_H}[{p_0}^h\chi(t)-p_1(t)]R^2(t)+\frac{1}{\eta_K}\int_0^t[{p_0}^h\chi(\tau)-p_1(\tau)]R^2(\tau)\exp^{-\frac{G_K}{\eta_K}(t-\tau)}d\tau\right\} \tag{35}$$

5.1 Solution for the first liner stage

Substituting Eq. (34) into Eq. (26), and defining $\varphi_1^B(t)=p_{11}(t)\exp^{\frac{G_K}{\eta_K}t}$ and $e_1=\dfrac{R_1G_H}{2G_Ha_{00}-R_1}$ the integral equation for $\varphi_1^B(t)$ can be obtained after simplification:

$$\begin{aligned}\varphi_1^B(t)=&\frac{e_1}{\eta_K}\int_{t_1}^t\varphi_1^B(\tau)d\tau+\frac{{p_0}^he_1}{G_H}\exp^{\frac{G_K}{\eta_K}t}[\chi(t_1)-\chi(t)]+\\&\frac{e_1{p_0}^h}{\eta_K{R_1}^2}\exp^{\frac{G_K}{\eta_K}(t-t_1)}\int_0^{t_1}\chi(\tau)R^2(\tau)\exp^{\frac{G_K}{\eta_K}\tau}d\tau-\frac{e_1{p_0}^h}{\eta_K{R_1}^2}\int_0^t\chi(\tau)R^2(\tau)\exp^{\frac{G_K}{\eta_K}\tau}d\tau\end{aligned} \tag{36}$$

Defining $\lambda_1^B=\dfrac{e_1}{\eta_K}$, and

$$f_1^B(t)=\frac{{p_0}^he_1}{G_H}\exp^{\frac{G_K}{\eta_K}t}[\chi(t_1)-\chi(t)]+\frac{e_1{p_0}^h}{\eta_K{R_1}^2}\exp^{\frac{G_K}{\eta_K}(t-t_1)}\int_0^{t_1}\chi(\tau)R^2(\tau)\exp^{\frac{G_K}{\eta_K}\tau}d\tau-\frac{e_1{p_0}^h}{\eta_K{R_1}^2}\int_0^t\chi(\tau)R^2(\tau)\exp^{\frac{G_K}{\eta_K}\tau}d\tau$$

Eq. (36) is a standard integral equation, that is:

$$\varphi_1^B(t)=\lambda_1^B\int_{t_1}^t k_1^B(t,\tau)\cdot\varphi_1^B(\tau)d\tau+f_1^B(t) \tag{37}$$

The kernel of this integral equation is $k_1^B(t,\tau)=1$, and the free term is $f_1^B(t)$. According to the theory of integral equations [30], the iterated kernel can be determined by iteration:

$$\begin{aligned}&k_{11}(t,\tau)=k_1^B(t,\tau)=1,\\&k_{12}(t,\tau)=\int_\tau^t k_1^B(t,u)\cdot k_{11}(u,\tau)du=t-\tau,\\&k_{13}(t,\tau)=\int_\tau^t k_1^B(t,u)\cdot k_{12}(u,\tau)du=(t-\tau)^2/2,\\&\cdots,\\&k_{1j}(t,\tau)=(t-\tau)^{j-1}/(j-1)!\end{aligned} \tag{38}$$

Accordingly, the kernel function is written as:

$$W_1^B(t,\tau,\lambda_1^B)=\sum_{j=1}^{\infty}\left(\lambda_1^B\right)^{j-1}k_{1j}(t,\tau)=\sum_{j=1}^{\infty}\left(\lambda_1^B\right)^{j-1}\frac{(t-\tau)^{j-1}}{(j-1)!}=\exp^{\lambda_1^B(t-\tau)} \tag{39}$$

Further, the solution for the integral equation can be expressed in analytical form as:

$$\varphi_1^B(t)=f_1^B(t)+\lambda_1^B\int_{t_1}^{t}W_1^B(t,\tau,\lambda_1^B)f_1^B(\tau)d\tau \tag{40}$$

Hence, the supporting pressure $p_{11}(t)$ in the first liner stage can be determined, so that displacements and stresses in the rock mass and the first liner can be calculated.

5.2 Solutions for the second liner stage

Substituting Eq. (34) into Eq. (29), and defining

$$\varphi_2^B(t)=p_{12}(t)\exp^{\frac{G_K}{\eta_K}t} \tag{41}$$

the integral equation for $\varphi_2^B(t)$ can be obtained after some manipulations:

$$\begin{aligned}\varphi_2^B(t)=&\frac{e_2}{\eta_K}\int_{t_2}^{t}\varphi_2^B(\tau)d\tau+\frac{e_2}{R_1^2}\left\{\frac{p_0^hR_1^2}{G_H}\exp^{\frac{G_K}{\eta_K}t}[\chi(t_1)-\chi(t)]+\frac{p_0^h}{\eta_K}\exp^{\frac{G_K}{\eta_K}(t-t_1)}\int_0^{t_1}\chi(\tau)R^2(\tau)\exp^{\frac{G_K}{\eta_K}\tau}d\tau\right.\\&\left.-\frac{p_0^h}{\eta_K}\int_0^{t}\chi(\tau)R^2(\tau)\exp^{\frac{G_K}{\eta_K}\tau}d\tau+\frac{R_1^2}{\eta_K}\int_{t_1}^{t_2}p_{11}(\tau)\exp^{\frac{G_K}{\eta_K}\tau}d\tau\right\}-\frac{2e_2a_{01}a_{10}}{a_{11}R_1}\exp^{\frac{G_K}{\eta_K}t}p_{11}(t_2)\end{aligned} \tag{42}$$

where $e_2=\dfrac{a_{11}G_HR_1}{2G_H(a_{00}a_{11}-a_{01}a_{10})-R_1a_{11}}$. If $\lambda_2^B=\dfrac{e_2}{\eta_K}$, and the free term $f_2^B(t)$:

$$\begin{aligned}f_2^B(t)=&\frac{e_2}{R_1^2}\left\{\frac{p_0^hR_1^2}{G_H}\exp^{\frac{G_K}{\eta_K}t}[\chi(t_1)-\chi(t)]+\frac{p_0^h}{\eta_K}\exp^{\frac{G_K}{\eta_K}(t-t_1)}\int_0^{t_1}\chi(\tau)R^2(\tau)\exp^{\frac{G_K}{\eta_K}\tau}d\tau\right.\\&\left.-\frac{p_0^h}{\eta_K}\int_0^{t}\chi(\tau)R^2(\tau)\exp^{\frac{G_K}{\eta_K}\tau}d\tau+\frac{R_1^2}{\eta_K}\int_{t_1}^{t_2}p_{11}(\tau)\exp^{\frac{G_K}{\eta_K}\tau}d\tau\right\}-\frac{2e_2a_{01}a_{10}}{a_{11}R_1}\exp^{\frac{G_K}{\eta_K}t}p_{11}(t_2)\end{aligned}$$

Eq. (42) is in the same format as the standard integral equation (Eq. (40)), so it can be rewritten as:

$$\varphi_2^B(t)=\lambda_2^B\int_{t_2}^{t}k_2^B(t,\tau)\cdot\varphi_2^B(\tau)d\tau+f_2^B(t) \tag{43}$$

with $k_2^B(t,\tau)=1$. Following the same procedure, the solution can be achieved:

$$\varphi_2^B(t)=f_2^B(t)+\lambda_2^B\int_{t_2}^{t}\exp^{\lambda_2^B(t-\tau)}f_2^B(\tau)d\tau \tag{44}$$

then $p_{12}(t)$ is determined from Eq. (57) and $p_{22}(t)$ by substituting $p_{12}(t)$ into Eq. (28).

5.3 Solution for the *i*-th liner stage

Substituting Eq. (34) into Eq. (30-1), leads to

$$
\begin{aligned}
&\frac{R_1}{2}\left\{\sum_{j=1}^{i-1}\left[\frac{1}{\eta_K}\int_{t_j}^{t_{j+1}} p_{1j}(\tau)\exp^{-\frac{G_K}{\eta_K}(t-\tau)}d\tau\right]+\frac{1}{G_H}p_{1i}(t)+\frac{1}{\eta_K}\int_{t_i}^{t} p_{1i}(\tau)\exp^{-\frac{G_K}{\eta_K}(t-\tau)}d\tau\right\}\\
&+\frac{1}{2R_1}\left\{\frac{p_0{}^h R_1{}^2}{G_H}\left[\chi(t_1)-\chi(t)\right]+\frac{p_0{}^h}{\eta_K}\int_0^{t_1}\chi(\tau)R^2(\tau)\exp^{-\frac{G_K}{\eta_K}(t_1-\tau)}d\tau-\frac{p_0{}^h}{\eta_K}\int_0^{t}\chi(\tau)R^2(\tau)\exp^{-\frac{G_K}{\eta_K}(t-\tau)}d\tau\right\} \qquad (45)\\
&=a_{00}p_{1i}(t)+a_{02}p_{2i}(t)
\end{aligned}
$$

According to Eq. (32), the supporting pressure $p_{2i}(t)$ in i-th stage can be expressed by $p_{1i}(t)$ as

$$
p_{2i}(t)=-a_{10}\frac{\boldsymbol{A}_{1,1}}{|\boldsymbol{A}|}p_{1i}(t)+\frac{1}{|\boldsymbol{A}|}\left[\sum_{j=1}^{i-1}a_{(j+1)j}\boldsymbol{A}_{j,1}p_{jj}(t_{j+1})\right] \qquad (46)
$$

where $|\boldsymbol{A}|$ is the determinant of $\boldsymbol{A}$, and $\boldsymbol{A}_{j,1}$ is the algebraic complement of the element a_{j1}. Substituting into Eq. (45) and simplifying, the equation for $p_{1i}(t)$ is as follows:

$$
\begin{aligned}
&p_{1i}(t)=\frac{e_i}{\eta_K}\int_{t_i}^{t} p_{1i}(\tau)\exp^{-\frac{G_K}{\eta_K}(t-\tau)}d\tau+e_i\sum_{j=1}^{i-1}\left[\frac{1}{\eta_K}\int_{t_j}^{t_{j+1}} p_{1j}(\tau)\exp^{-\frac{G_K}{\eta_K}(t-\tau)}d\tau\right]\\
&+\frac{e_i}{R_1^2}\left\{\frac{p_0{}^h R_1{}^2}{G_H}\left[\chi(t_1)-\chi(t)\right]+\frac{p_0{}^h}{\eta_K}\int_0^{t_1}\chi(\tau)R^2(\tau)\exp^{-\frac{G_K}{\eta_K}(t_1-\tau)}d\tau-\frac{p_0{}^h}{\eta_K}\int_0^{t}\chi(\tau)R^2(\tau)\exp^{-\frac{G_K}{\eta_K}(t-\tau)}d\tau\right\} \qquad (47)\\
&-\frac{2a_{01}e_i}{R_1}\left\{\frac{1}{|\boldsymbol{A}|}\left[\sum_{j=1}^{i-1}a_{(j+1)j}\boldsymbol{A}_{j,1}p_{jj}(t_{j+1})\right]\right\}
\end{aligned}
$$

where $e_i=\dfrac{G_H R_1}{2G_H(a_{00}-a_{01}a_{10}c_i)-R_1}$ and $c_i=\dfrac{\boldsymbol{A}_{1,1}}{|\boldsymbol{A}|}$. Let $\varphi_i^B(t)=p_{1i}(t)\exp^{\frac{G_K}{\eta_K}t}$, integral equation for $\varphi_i^B(t)$ can be obtained after simplification,

$$
\begin{aligned}
&\varphi_i^B(t)=\frac{e_i}{\eta_K}\int_{t_i}^{t}\varphi_i^B(\tau)d\tau+e_i\sum_{j=1}^{i-1}\left[\frac{1}{\eta_K}\int_{t_j}^{t_{j+1}} p_{1j}(\tau)\exp^{\frac{G_K}{\eta_K}\tau}d\tau\right]-\frac{2a_{01}e_i}{R_1}\exp^{\frac{G_K}{\eta_K}t}\left\{\frac{1}{|\boldsymbol{A}|}\left[\sum_{j=1}^{i-1}a_{(j+1)j}\boldsymbol{A}_{j,1}p_{jj}(t_{j+1})\right]\right\}\\
&+\frac{e_i}{R_1^2}\left\{\frac{p_0{}^h R_1{}^2}{G_H}\exp^{\frac{G_K}{\eta_K}t}\left[\chi(t_1)-\chi(t)\right]+\frac{p_0{}^h}{\eta_K}\exp^{\frac{G_K}{\eta_K}(t-t_1)}\int_0^{t_1}\chi(\tau)R^2(\tau)\exp^{\frac{G_K}{\eta_K}\tau}d\tau-\frac{p_0{}^h}{\eta_K}\int_0^{t}\chi(\tau)R^2(\tau)\exp^{\frac{G_K}{\eta_K}\tau}d\tau\right\}
\end{aligned} \qquad (48)
$$

If $\lambda_i^B=\dfrac{e_i}{\eta_K}$, and the free term $f_i^B(t)$:

$$
\begin{aligned}
&f_i^B(t)=e_i\sum_{j=1}^{i-1}\left[\frac{1}{\eta_K}\int_{t_j}^{t_{j+1}} p_{1j}(\tau)\exp^{\frac{G_K}{\eta_K}\tau}d\tau\right]-\frac{2a_{01}e_i}{R_1}\exp^{\frac{G_K}{\eta_K}t}\left\{\frac{1}{|\boldsymbol{A}|}\left[\sum_{j=1}^{i-1}a_{(j+1)j}\boldsymbol{A}_{j,1}p_{jj}(t_{j+1})\right]\right\}\\
&+\frac{e_i}{R_1^2}\left\{\frac{p_0{}^h R_1{}^2}{G_H}\exp^{\frac{G_K}{\eta_K}t}\left[\chi(t_1)-\chi(t)\right]+\frac{p_0{}^h}{\eta_K}\exp^{\frac{G_K}{\eta_K}(t-t_1)}\int_0^{t_1}\chi(\tau)R^2(\tau)\exp^{\frac{G_K}{\eta_K}\tau}d\tau-\frac{p_0{}^h}{\eta_K}\int_0^{t}\chi(\tau)R^2(\tau)\exp^{\frac{G_K}{\eta_K}\tau}d\tau\right\}
\end{aligned}
$$

the Eq. (49) is a same format standard integral equation as the above, that is,

$$\varphi_i^B(t) = \lambda_i^B \int_{t_i}^{t} k_i^B(t,\tau) \cdot \varphi_i^B(\tau) d\tau + f_i^B(t) \tag{49}$$

and $k_i^B(t,\tau) = 1$. Solving process is established to obtain the solution which is

$$\varphi_i^B(t) = f_i^B(t) + \lambda_i^B \int_{t_i}^{t} \exp^{\lambda_i^B(t-\tau)} f_i^B(\tau) d\tau \tag{50}$$

all the equations and solutions of the supporting pressures are obtained by replacing 'i' with 2, then 3, then 4, in turn until *n*.

6 Parametric investigation

In order to illustrate the effect of the rock viscoelastic constants, of the excavation process, of the mechanical and geometrical properties of the liners and of their installation times on the ground displacements and supporting pressures, a parametric study for a support made of three liners installed in succession has been carried out. The use of three liners installed at different times is becoming increasingly more popular in tunnel construction: [311] describes the installation of steel sets (first), backfilled chemical grouting (second), and a final concrete liner in a mine tunnel; [32] describes the installation of steel sets (first), concrete slabs laid in between (second) and the final concrete liner; [22] investigates the use of 2 thin sprayed-on liners part of a support system of at least 3 liners (the final concrete liner typically being cast after some time). To investigate the influence of the several parameters involved, they were varied in turn: first we analyzed the influence of the rock rheological parameters (§ 6.1), then the speed of radial excavation (§ 6.2), the speed of longitudinal advancement (§ 6.3), the time of installation of the liners (§ 6.4), and the liner thicknesses (§ 6.5) and shear moduli (§ 6.6).

Concerning the excavation process, a linear increase of the tunnel radius over time was assumed: $g(t) = \mathrm{v}_r \cdot t$ (see Eq.(2)) with v_r the (constant) speed of excavation in the radial direction. It is now convenient to express Eq. (3) in dimensionless form:

$$\frac{R(t)}{R_{fin}} = \begin{cases} \dfrac{R_{ini}}{R_{fin}} + \dfrac{\mathrm{v}_r}{R_{fin}} t & 0 \le t \le t_0 \\ 1 & t > t_0 \end{cases} \tag{51}$$

Let us define the dimensional parameter $T_K = \eta_K / G_K$, expressing the retardation time of the Kelvin component of the generalized Kelvin model. It is convenient to express the speed of excavation in the radial direction in dimensionless form. To this end, we introduce n_r, defined as:

$$n_r = \mathrm{v}_r \cdot T_K / R_{fin} \tag{52}$$

so that the radius can now be expressed as:

$$\frac{R(t)}{R_{fin}} = \begin{cases} \frac{R_{ini}}{R_{fin}} + n_r \frac{t}{T_K} & 0 \le \frac{t}{T_K} \le \frac{t_0}{T_K} \\ 1 & \frac{t}{T_K} > \frac{t_0}{T_K} \end{cases} \tag{53}$$

Note that other choices would have been equally acceptable (for instance $n_r^* = \mathrm{v}_r \cdot t_0 / R_{fin}$). Also we assume a constant speed of advancement of the tunnel, i.e. v_l=*const*. It is convenient to express the speed of advancement in dimensionless form too:

$$n_l = \mathrm{v}_l \cdot T_K / R_{fin} \tag{54}$$

It is straightforward to observe that the ratio between the two speeds is constant: $\frac{\mathrm{v}_l}{\mathrm{v}_r} = \frac{n_l}{n_r}$.

We now need to determine a suitable expression for the function $\chi(t)$ accounting for the tunnel face effect on nearby sections. In [33], the following expression, derived from FEM simulations, was proposed:

$$\chi_1(t) = 1 - 0.7 \exp^{-m_1 \cdot x}, \tag{55}$$

with $m_1 = \frac{1.58}{R}$ and x being the longitudinal distance of the section considered to the tunnel face which in turn is a function of the tunnel advancement rate, with

$$x = x(t) = \mathrm{v}_l \cdot t \tag{56}$$

Panet and Guenot [34] suggested a different empirical relationship:

$$\chi_2(t) = 0.28 + 0.72 \left[1 - \left(\frac{m_2}{m_2 + x(t)} \right)^2 \right], \tag{57}$$

with $m_2 = 0.84R$. The consideration of sequential excavation implies that the tunnel radius R varies along the longitudinal direction, from R=R_{ini} at the tunnel face (x=0), to R=R_{fin} at a distance x^* from the tunnel face. This distance is a function of the $\mathrm{v}_l/\mathrm{v}_r$ ratio (see Figure 3c) and can be obtained from Eqs. (53), (54) and (56):

$$x^* = \frac{\mathrm{v}_l}{\mathrm{v}_r}\left(R_{fin} - R_{ini}\right) \tag{58}$$

In Figure 3a, a visual comparison between the two proposed expressions for some values of the ratio $\mathrm{v}_l/\mathrm{v}_r$ is provided. From the figure it emerges that the two proposed expressions are very similar. Since the expression in Eq. (57) cannot be integrated analytically, we decided to adopt the expression of Eq. (55) which instead can be analytically integrated easily. Note that unlike the case of instantaneous radial excavation considered by Panet and Guenot [34], a small approximation in the calculation of χ is here introduced because the expression proposed by Panet and Guenot [34] is based on the assumption of constant tunnel radius, whereas in our case, for $x<x^*$ (i.e. from the considered section to the tunnel face), R reduces progressively from R_{fin} to R_{ini} (see Figure 3~~b~~).

So in case of a linear increase of the tunnel radius over time, as assumed in Eq. (51), and assuming $\chi = \chi_1(t)$ (see Eq. (55)) to account for the tunnel face advancement effect, closed-form analytical expressions for radial displacements and supporting pressure on the rock can be derived. These (lengthy) expressions are reported in Appendix A for all the stages of the excavation process. Instead, in case of non-linear increase of the tunnel radius over time (i.e. a non-linear function $\psi = \psi(t)$ in Eq.(2)), and/or $\chi \neq \chi_1(t)$, the solutions will likely cease to be closed-form. However, if $\int \chi(\tau) R^2(\tau) \exp^{\frac{G_K}{\eta_K}\tau} d\tau$ and the integrals in Eqs. (40), (44) and (50) can be integrated analytically, closed form analytical solutions can still be obtained.

6.1 Influence of the material parameters on tunnel convergence and stresses

In Figure 4, the normalized tunnel convergence u_r / u_r^∞ is plotted against time normalized by the final time of excavation, t/t_0, for different values of the rheological parameters of the rock. The final radial displacement without considering sequential excavation, i.e. assuming instantaneous excavation in the radial direction, and without any support is:

$$u_r^\infty = \frac{p_0{}^h R_1{}^2}{2r}\left(\frac{1}{G_H} + \frac{1}{G_K}\right) \qquad (59)$$

The values assumed for all the other geometrical and mechanical parameters of the liners are shown in Table 1. Concerning the excavation process, the following values were assumed: $R_{ini} = 1/6\,R_{fin}$, $\mathrm{v}_r = \frac{5}{6}\frac{R_{fin}}{t_0}$ and $\mathrm{v}_l = \frac{5}{4}\frac{R_{fin}}{t_0}$. Considering fixed ratios of G_K/G_H (curves 1,4,5 or 2,6,8 or 3,7,9 in Figure 4a), it can be observed that the larger the value~~s~~ of T_K/t_0, the smaller is the radial convergence and the larger is the time needed to reach the final convergence which in turn is smaller, i.e. the horizontal asymptotes of the curves become lower for increasing T_K. It can also be observed that for small values of T_K, most of the displacement occurs during the excavation stage because of the fast rheological flow in the rock. In Figure 4(b) and (c), radial and hoop stresses respectively at the interface between rock and first liner are plotted against time. With regard to the radial stress, we can observe that it decreases during the excavation stage but increases after the support system is installed. For large values of T_K/t_0 (with the same ratios of G_K/G_H), the final radial stress is larger whereas the final hoop stress is smaller. As it can be expected the variation of the hoop stress over time is opposite to the variation of the radial stress, i.e. when the radial stress decreases, the hoop stress increases and vice versa. Looking at both displacements and stresses, it emerges that at the limit, for $T_K \to 0$, the installation of the liners does not make any significant difference since the viscosity induced displacements occurring after the excavation are negligible. Considering now, curves obtained for the same values of T_K/t_0 (for example 1,2,3 or 4,6,7 or 5,8,9), it can be observed that for high values of G_K/G_H, the radial displacements are larger and reach their final asymptotic value earlier, the normalized radial stresses are smaller, and the hoop stresses are larger. Considering the two parameters, T_K/t_0 and G_K/G_H, it can be observed that T_K/t_0 influences the rate of convergence and stress change occurring over time: for low values of T_K/t_0, large displacements take place in the first phase with the final state being reached earlier. Instead, G_K/G_H affects the proportion of displacements or stresses independent of time, with the elastic displacements and stresses being larger for increasing G_K/G_H.

When G_K=0, the Maxwell model is obtained. In this case, according to Eq. (59), in the absence of support, $u_r^\infty \to \infty$, and $T_K \to \infty$. Hence, in order to normalize the displacements, a different normalization has to be employed. To this end, we chose to use the initial (at completion of excavation) elastic displacement in case of instantaneous radial and longitudinal excavation (no tunnel face effect): $u_r^0 = \dfrac{p_0{}^h R_1^2}{2G_H r}$. In Figure 5 the normalized displacement, radial and hoop stresses are plotted against the time normalized by the excavation time for various values of the relaxation time T_M of the Maxwell model with $T_M = \eta_K/G_H$. It emerges that larger ratios of T_M/t_0 correspond to smaller convergence and slow rheological flow in the rock. Also looking at the variation of the stresses over time (see Figure 5b and c) it can be observed that for large T_M/t_0, radial stress and hoop stress undergo smaller variations over time.

6.2 Influence of the radial excavation rate

In the following figures, time has been normalized by the retardation time of the Kelvin component of the model: t/T_K. To investigate the influence of the radial excavation rate, five values of n_r, the dimensionless radial excavation speed (see Eq.(52)), were adopted: (1) $n_r = \frac{5}{9}$ (implying $\frac{t_0}{T_K} = \frac{3}{2}$); (2) $n_r = \frac{5}{6}$ (implying $\frac{t_0}{T_K} = 1$); (3) $n_r = \frac{5}{3}$ (implying $\frac{t_0}{T_K} = \frac{1}{2}$); (4) $n_r = \frac{20}{3}$ (implying $\frac{t_0}{T_K} = \frac{1}{8}$) and (5) $n_r \to \infty$ corresponding to the case of instantaneous radial excavation ($\frac{t_0}{T_K} = 0$).The first liner is installed immediately after radial excavation, that is, $t_1 = t_0$, with the second and third liner installed at $t_2 = t_0 + \frac{1}{4}T_K$ and $t_3 = t_0 + \frac{3}{4}T_K$, respectively. The values assumed for all the other geometrical and mechanical parameters of the liners are shown in Table 1. In Figure 6 the curves of normalized displacements are plotted against the normalized time for three types of rock (various values of G_K/G_H). The symbol '•' represents the end time of excavation, t_0, i.e. when the full cross section is excavated. For the case of high radial excavation speed, the displacement occurring during the supporting stages is significant and in case of low values of G_K, is more than the displacement occurring during the excavation process. In this case, it can be observed that the longitudinal advancement has a strong effect on the observed displacements also after the installation of the support. It can also be noted that progressively larger values of G_K/G_H imply a smaller influence of the excavation process on the state of displacement of the rock.

In Figure 7, the normalized stresses calculated at the interface between rock and the first liner r=R_1, are plotted. It can be observed that at the end of the excavation, lower excavation speeds imply a smaller radial stress and a larger circumferential one, hence larger stresses in the rock. Looking at Eq. (12), it emerges that the stresses during the excavation stage depend only on the size of the opening and on the parameter χ. So the stress differences exhibited at time t_0 in Figure 7 are entirely ascribable to the different distances of the considered section to the tunnel face which in turn is a function of the radial excavation speed. In case of lower excavation speed (curves 1 and 2 in Figure 7), the radial and circumferential stresses reach their minimum and maximum values respectively at the end of the excavation process, with the radial stress increasing and the circumference one decreasing after the installation of the first liner. Finally, as it has already been observed for radial convergence, it emerges that large values of G_K/G_H imply a smaller influence of the excavation process on the state of stress of the rock.

In Figure 8, the normalized radial convergence and stresses against time normalized by the relaxation time T_M of the Maxwell model, are plotted for the Maxwell model. In comparison with the generalized Kelvin model, the trends exhibited are similar, with the quantitative variation over time being remarkably significant.

6.3 Influence of the advancement rate (longitudinal excavation rate)

In this section, the parameters employed for the supporting system, construction process and the excavation size are the same as in section 6.2 (see table 1). The normalized distance between the examined section and the tunnel face can be written as:

$$\frac{x(t)}{R_{fin}} = n_l \frac{t}{T_K} \tag{60}$$

In Figure 9 the normalized displacement, circumferential and radial stresses are plotted against t/T_K for various advancement rates: (1) $n_l = \infty$ representing the ideal case of instantaneous tunnel advancement; (2) $n_l = \frac{10}{3}$; (3) $n_l = 2$; (4) $n_l = \frac{2}{3}$. Also two different normalized cross-section excavation rates were considered: $n_r = \frac{20}{3}$ and $n_r = \frac{5}{3}$. Concerning the rock properties, $G_K/G_H = 1$ was assumed. When the radial excavation speed is high, (see Figure 9a), radial convergence and stresses are more sensitive to the speed of longitudinal advancement. The differences between the curves obtained for various speeds of longitudinal advancement in Figure 9a for a high cross-section excavation rate are significantly higher than the differences exhibited in Figure 9b by the curves achieved for a low cross-section excavation rate, especially for the three cases with higher speed of longitudinal advancement. This is also true for the displacement and stresses at the end of the excavation process and for $t \to \infty$. For this reason, in tunnel construction, advancement rates should be designed according to the foreseen cross-section excavation rate. In case of high sectional excavation speed, a variable advancement speed can be adopted in order to control either radial convergence or stresses; whilst in case of low sectional excavation speed, the influence of the longitudinal advancement rate on the tunnel response is significantly less.

6.4 Influence of the time of liner installation

The function of the support is to provide the supporting pressure to the tunnel opening to prevent any rock wedge failure and limit the amount of rock convergence. The larger the supporting pressure is, the smaller the radial convergence is. According to Eqs. (40), (44) and (50), the amount of supporting pressure p_1 depends on the radial excavation process. In Figure 10 the variation of p_1 for different excavation rates but the same time intervals between the installation times of the liners is plotted against the normalized relative time $(t-t_1)/T_k$. Two times of end radial excavation were considered: $\frac{t_0}{T_K}=\frac{1}{8}$ (curves 1 and 3) and $\frac{t_0}{T_K}=\frac{1}{2}$ (curves 2 and 4). In case of curves 1 and 2, the first liner is installed immediately at the end of the excavation, i.e. $(t_1-t_0)/T_k=0$. Instead, in case of curves 3 and 4, the installation time of the first liner is $(t_1-t_0)/T_k=1$. It can be observed that the pressure p_1 increases with time reaching an asymptotic value in all the cases. Now, if we compare curves obtained for the same installation times of the second and third liners, but with the installation time of the first liner being different (curve 1 with 3 and curve 2 with 4), it emerges that early installation of the first liner leads to a larger support pressure, with the difference between curves 1 and 3 being significantly higher than the difference between curves 2 and 4. This means that for higher excavation speeds, the influence of the installation time of the liner is larger. Finally, comparing curve 1 with 2 (and analogously curve 3 with 4), the normalized relative time of installation of the first liner, $(t_1-t_0)/T_k$, is the same, but the end time of excavation, t_0, is different, so it can be concluded that the supporting pressure is larger when the tunnel is excavated faster.

Now, in order to study the influence of the installation times of all the three liners, we assumed the following parameters: $\chi(t)=1$, $\frac{t_0}{T_K}=\frac{1}{8}$ and $\frac{G_K}{G_H}=1$, with the material parameters of liners shown in Table 1. In Figure 11 the variation of the support pressure p_1 for various first, second and third liner installation times is plotted against time. From Figure 11a it emerges that being fixed the installation times of the second and third liner, the earlier the first liner is applied, the larger the final supporting pressure is. In Figure 11b the pressure is plotted against the time interval since installation of the first liner. It emerges that the supporting pressure p_1 changes little until the time

${(t-t_1)}/{T_K} = 1.0$. Then, in case of an early installation of the first liner, it increases rapidly; whereas in case of a late installation the pressure is smaller and reaches an asymptotic value earlier.

In Figure 11c and d, the influence of the times of installation of the second and third liners is investigated by plotting curves for various installation times. The time intervals between the installation of the first and second liner (curves in Figure 11c) and between the second and third liner (curves in Figure 11d) is the same as the time difference between the end of excavation and the installation of the first liner in Figure 11a and b. Once again it emerges that when liners are installed early, the pressure is larger whereas liners installed at later times lead to smaller pressure and less differences among the curves. So it can be concluded that later installation times make the support pressure becoming progressively less sensitive to the installation times themselves.

6.5 Influence of the thickness of the liners

The influence of liner thickness has been investigated by [21] for the case of a single liner where it has been shown that higher thicknesses are beneficial to reduce the convergence of the tunnel. However, beyond certain values, increasing the thickness ceases to be a viable economic option to reduce tunnel convergence. Here, we consider a constant total thickness for the support system made of 3 liners, $d_{tot}=d_1+d_2+d_3$, and investigate the effect of adopting different relative thicknesses between the 3 liners on tunnel convergence, i.e. how much convergence reduction can be achieved by optimizing the distribution of the support thickness among the liners. In Figure 12b, the curves of displacement and supporting pressure obtained for four different cases are plotted. It can be observed that trends in terms of radial convergence (Fig. 12a) are mirrored by the trends in terms of support pressure (Fig. 12b): the combinations of thicknesses giving rise to the lower radial convergences are associated to the higher support pressures and vice versa the combinations giving rise to the higher convergences are associated to the lower radial convergences with the order between curves being reversed. Curves 1, 2 and 4 refer to two liners having the same thickness with one liner being twice as thick whereas curve 3 refers to the case of liners of refers to the case of equal thickness. It emerges that the best choice to reduce convergence is to assign the highest thickness to the first liner. It also emerges that given a target in terms of radial convergence and support pressure, there is more than one combination of thicknesses among liners that can be adopted so that the designer has a certain flexibility in the choice and the choice can be made in the light of other considerations (e.g. technological efficiency and cost reduction).

6.6 Influence of the elastic shear moduli of the liners

In the case here considered of 3 liners of equal thickness, the average shear modulus can be calculated simply as $G_L = \frac{G_1^L + G_2^L + G_3^L}{3}$. The rock response is a function of the modular ratio $n_s = \frac{G_L}{G_\infty}$ between liners and rock, where $G_\infty = \frac{G_H G_K}{G_H + G_K}$ is the long term shear modulus of the rock. In Figure 13, radial convergence and supporting pressure are plotted against time for various values of the modular ratio n_s, with the thickness and shear modulus of each liner being the same ($\frac{d_i}{R_1} = \frac{1}{60}, i = 1,2,3$) and $\frac{t_0}{T_K} = \frac{t_1}{T_K} = \frac{1}{8}$, $\frac{t_2}{T_K} = \frac{1}{2}$, $\frac{t_3}{T_K} = 1$. From the figure it emerges that high values of n_s lead to smaller radial convergence and higher support pressure. However, the rates of decrease of radial convergence and increase of support pressure progressively reduce with n_s increasing. In Figure 14b, the influence of the relative shear modulus between liners is investigated with $n_s = 20$. In the figure, radial convergence and supporting pressure are plotted for various values of relative modulus between liners but all with the same average shear modulus G_L. It emerges that convergence is biggest when G_3^L (shear modulus of the third liner) is largest. The curves obtained for $G_1^L = G_3^L$ (curve 1,4,5), exhibit similar trends. So the most efficient way to reduce convergence is to increase the shear modulus of first liner.

7 Application example

In this section, the presented solutions are employed for the prediction of the convergence and support pressure in a circular tunnel recently excavated in China (Shilong tunnel in Sichuan province [35]), where three liners have been used. The tunnel was excavated at a depth of 300 meters, in mudstone and/or sandstone, with the rock bulk unit weight being $\gamma = 26.3kN/m^3$. The tunnel was subject to a hydrostatic initial stress of $p_0^h = 7.9MPa$. According to experimental tests and back analysis [35], the following rock parameters can be assumed: $G_K = 458MPa$, $G_H = 550MPa$, $\eta_K = 4000MPa \cdot day$. A pilot tunnel of radius $R_{ini} = 1.8m$ was first excavated, then after 1 day enlarged to a final radius of $R_{fin} = 6.2m$. Therefore, the variation of the excavation radius over time can be expressed analytically as follows:

$$R(t)=\begin{cases}1.8 & 0\le t<1\\ 6.2 & t\ge 1\end{cases}\ \text{(unit: m)} \tag{61}$$

A first liner of shotcrete was installed (sprayed) 1 day after excavation. Then, steel sets were put in place with shotcrete sprayed immediately afterwards. Steel sets and shotcrete are here treated as a single composite liner. After some days, the final (third) concrete liner was installed. In table 2 the properties of the materials employed for the support are provided together with the sectional properties of the composite liner made of steel sets and shotcrete which were calculated according to [32].

In order to showcase the enhancement obtained in the accuracy of the calculation of the tunnel response due to the solution proposed in this paper, we carried out two calculations: in the first one the support is considered made of all its liners (3) whilst in the second one the support was considered made of 2 liners that is the maximum number of liners for which the analytical solution in [26] can be utilized. Comparison of the tunnel response in terms of radial convergence and stress field between the responses predicted by the two calculations provides a quantitative estimation of the importance that considering the actual number of liners may have. In case of the latter calculation, the first and second liners were considered as one single liner. The equivalent modulus for this liner was calculated as follows:

$$\bar{E}_L=\frac{E_1^L d_1+E_2^L d_2}{d_1+d_2} \tag{62}$$

with the thickness of the liner taken as $\bar{d}_L=d_1+d_2$.

In Figure 15, the mechanical response at the interface between the first liner and the surrounding rock (r=6.2m) is plotted against time, for the two cases considered: 3 liners, calculated according to the solution presented in this paper with the second liner installed at various times (t_2= 1 day; 2 days; 3 days; 8 days), and 2 liners, calculated according to [26] which is identified by the red curves in the plotted charts (corresponding to the case t_2=t_1). From Figure 15a, it emerges that the radial convergence calculated considering three liners is larger than the convergence obtained for the two liner system, the radial stress is smaller whereas the hoop stress is larger. The largest difference in terms of either final convergence or stresses is observed when the second liner is installed at the latest time considered (t_2=8 days). With regard to the radial convergence, the difference is 12mm corresponding to 23% of the final convergence calculated for a 2 liner system. With regard to radial stresses, the difference is around 1 MPa corresponding to 29% of the final value of radial stress calculated for a 2 liner system. These differences are non negligible from an engineering point of view. Therefore, from this example, it emerges that predictions of the mechanical response of a three liner tunnel excavated in viscoelastic rock made using the currently available analytical solution for a 2 liner system, [26], can be subject to a significant error that can be avoided by using the solution illustrated in this paper for support systems made of any number of liners.

8 Conclusions

The main factors for the observed time dependency in tunnel construction are due to the sequence of excavation, the number of liners and their times of installation and the rheological properties of the host rock. A general analytical solution accounting for all the three factors has been derived for the first time. The solution was derived for the generalized Kelvin viscoelastic model and for the Maxwell one as a particular case. The integral equations for the supporting pressures were established according to time-dependent boundary conditions. Explicit closed form analytical expressions for the time-dependent supporting pressures, stresses and displacements in the rock and the liners were obtained by solving the established integral equations. The obtained solution has been derived for a circular tunnel supported by a generic number of liners installed at various times each one of different thickness and shear modulus. Sequential excavation was accounted for assuming the radius of the tunnel growing from an initial value to a final one according to a time dependent function to be prescribed by the designer. The effect of tunnel advancement was also considered.

An extensive parametric study for a support system made of 3 liners was performed investigating the influence of the excavation process adopted, the rheological properties of the rock, shear modulus, thickness and installation times of the liners on radial convergence, support pressures and the stress field in the rock. Several dimensionless charts for ease of use of practitioners are provided in the paper. From the study, it emerges that:

- Large values of the ratio between the characteristic time of the Kelvin component of the generalized Kelvin model and the total excavation time in the considered cross-section, T_K/t_0, imply smaller radial convergence with more time needed to reach the final displacement, whereas for small values of T_K/t_0 (fast rheological flow in the rock), most of the displacement occurs during the excavation stage. Large values of the ratio between the Kelvin and the

Hookean shear moduli, G_K/G_H, imply larger radial convergences;

- T_K/t_0 has stronger influence on the displacements than G_K/G_H;
- in case of low radial excavation speed, significant displacements are observed during the excavation stages, with the radial and circumferential stresses reaching their minimum and maximum values respectively at the end of the excavation process;
- progressively larger values of G_K/G_H imply a smaller influence of the excavation process on the observed displacements;
- radial convergence and stresses are sensitive to the speed of longitudinal advancement especially for high radial excavation speeds. For this reason, in tunnel construction, advancement rates should be designed according to the foreseen cross-section excavation rate;
- the influence of the installation time of the liners is larger for higher excavation speeds;
- there is more than one combination of thicknesses among liners that leads to the same target radial convergence and support pressure;
- the shear modulus and thickness of the first liner bear the largest influence on the response of the tunnel in terms of radial convergence and support pressure in comparison with the other two liners.
- an example of a tunnel lined by 3 liners is illustrated. Calculations for an equivalent support system of 2 liners according to current literature provide values which may be significantly far from the values found accounting for the presence of all the liners so that it can be stated that consideration of the right number of liners is important to obtain realistic prediction of the tunnel response.

The obtained solutions are rigorously valid only in axisymmetric plane-strain conditions. However, according to the recent work of [27], the solutions are meaningful for a much wider range of ground conditions and for several cases of non-circular tunnels.

Acknowledgements

This work is supported by Major State Basic Research Development Program of China (973 Program) with Grant No.2014CB046901, Marie Curie Actions—International Research Staff Exchange Scheme (IRSES): GEO—geohazards and geomechanics with Grant No. 294976, National

Natural Science Foundation of Shanghai City with Grant No. 11ZR1438700, China National Funds for Distinguished Young Scientists with Grant No. 51025932, and National Natural Science Foundation of China with Grant No.51179128. These supports are greatly appreciated. The authors thank the reviewers for the valuable comments and suggestions for improving the presentation of the paper.

Appendix A. Closed form analytical expressions for radial displacement and supporting pressure for the generalized Kelvin viscoelastic model

In the following derivation, the rock is assumed to obey the generalized Kelvin viscoelastic model (see Fig. 2a), the tunnel radius is assumed to increase linearly over time (see Eq. (51)), and the function accounting for the effect of tunnel face advancement, $\chi(t)$, is assumed to be $\chi=\chi_1(t)$ (see Eq. (55)).

When $t<t_0$, i.e. during the excavation stage, the radial displacement is provided by Eq. (35). Substituting $p_1(t)=0$, Eqs. (51) and (55) into Eq. (35), the following expression is obtained:

$$\begin{aligned} u_{r1}(r,t) &= -\frac{p_0^h}{2r}\left\{\frac{1}{G_H}\chi(t)R^2(t)+\frac{1}{\eta_K}\exp^{-\frac{G_K}{\eta_K}t}\int_0^t\chi(\tau)R^2(\tau)\exp^{\frac{G_K}{\eta_K}\tau}d\tau\right\}= \\ &= -\frac{p_0^h}{2r}\left\{\frac{1}{G_H}\chi_1(t)\left(R_{ini}+\mathrm{v}_r t\right)^2+\frac{1}{\eta_K}\exp^{-\frac{G_K}{\eta_K}t}D_1(t)\right\} \end{aligned} \tag{A1}$$

where:

$$\begin{aligned} D_1(t) &= \int_0^t\chi(\tau)R^2(\tau)\exp^{\frac{G_K}{\eta_K}\tau}d\tau = -\frac{2v^2\eta_K{}^3}{G_K{}^3}+\frac{1.4v^2\eta_K{}^3R_{fin}{}^3}{G_K{}^3R_{fin}{}^3-4.73G_K{}^2\eta_K R_{fin}{}^2v_l+7.44G_K\eta_K{}^2R_{fin}v_l{}^2-3.91\eta_K{}^3v_l{}^3} \\ &+R_{ini}{}^2\left(-\frac{\eta_K}{G_K}+\frac{0.7\eta_K R_{fin}}{G_K R_{fin}-1.58\eta_K v_l}\right)+\exp^{-\frac{(R_{ini}+v_r t)(-G_K R_{fin}+1.58\eta_K v_l)}{v_r\eta_K R_{fin}}}\eta_K\Bigg(\frac{1}{G_K{}^3}\exp^{\frac{1.58\eta_K v_l v_r t+R_{ini}(-G_K R_{fin}+1.58\eta_K v_l)}{v_r\eta_K R_{fin}}} \\ &\left(v_r{}^2(G_K{}^2t^2-2G_K\eta_K t+2\eta_K{}^2)+G_K v_r(2G_K t-2\eta_K)R_{ini}+G_K{}^2R_{ini}{}^2\right) \\ &-\frac{0.7\exp^{-\frac{R_{ini}(G_K R_{fin}-1.58\eta_K v_l)}{v_r\eta_K R_{fin}}}(R_{ini}+v_r t)^2R_{fin}}{G_K R_{fin}-1.58\eta_K v_l}-\frac{1.4\exp^{-\frac{R_{ini}(G_K R_{fin}-1.58\eta_K v_l)}{v_r\eta_K R_{fin}}}v_r{}^2\eta_K{}^2R_{fin}{}^3}{(G_K R_{fin}-1.58\eta_K v_l)^3} \\ &+\frac{1.4\exp^{-\frac{R_{ini}(G_K R_{fin}-1.58\eta_K v_l)}{v_r\eta_K R_{fin}}}v_r\eta_K(R_{ini}+v_r t)R_{fin}{}^2}{(G_K R_{fin}-1.58\eta_K v_l)^2}\Bigg)+v_r\eta_K{}^2R_{ini}\left(\frac{2}{G_K{}^2}-\frac{1.4R_{fin}{}^2}{G_K{}^2R_{fin}{}^2-3.15G_K\eta_K R_{fin}v_l+2.48\eta_K{}^2v_l{}^2}\right) \end{aligned} \tag{A2}$$

The definition of all the coefficients can be found in Sections 3, 4 and 5.

When $t_0\le t<t_1$, i.e. the time after excavation before installation of the support, the radial displacement is provided by Eq. (35). Substituting $p_1(t)=0$, Eqs. (51) and (55) into Eq. (35), the radial displacement is obtained:

$$\begin{aligned} u_{r2}(r,t) &= -\frac{p_0^h}{2r}\left\{\frac{1}{G_H}\chi_1(t)R_{fin}{}^2+\frac{1}{\eta_K}\exp^{-\frac{G_K}{\eta_K}t}\int_0^{t_0}\chi(\tau)R^2(\tau)\exp^{\frac{G_K}{\eta_K}\tau}d\tau+\frac{1}{\eta_K}\exp^{-\frac{G_K}{\eta_K}t}R_{fin}{}^2\int_{t_0}^t\chi(\tau)\exp^{\frac{G_K}{\eta_K}\tau}d\tau\right\}= \\ &= -\frac{p_0^h}{2r}\left\{\frac{1}{G_H}\chi_1(t)R_{fin}{}^2+\frac{1}{\eta_K}\exp^{-\frac{G_K}{\eta_K}t}D_1(t_0)+\frac{1}{\eta_K}\exp^{-\frac{G_K}{\eta_K}t}R_{fin}{}^2D_2(t)\right\} \end{aligned} \tag{A3}$$

where:

$$D_2(t)=\int_{t_0}^{t}\chi(\tau)\exp^{\frac{G_K}{\eta_K}\tau}d\tau=\frac{\eta_K}{G_K}(\exp^{\frac{G_K}{\eta_K}t}-\exp^{\frac{G_K}{\eta_K}t_0})-\frac{0.7\eta_K R_{fin}}{G_K R_{fin}-1.58\eta_K v_l}(\exp^{\frac{G_K R_{fin}-1.58v_l\eta_K}{\eta_K R_{fin}}t}-\exp^{\frac{G_K R_{fin}-1.58v_l\eta_K}{\eta_K R_{fin}}t_0})\quad\text{(A4)}$$

When $t_1 \le t < t_2$, i.e. during the first liner stage, the support pressure acting on the rock is obtained by substituting Eq. (39). into Eq. (40) and $p_{11}(t)=\varphi_1^B(t)\exp^{-\frac{G_K}{\eta_K}t}$ obtaining:

$$\begin{aligned}p_{11}(t)=&e_1 p_0{}^h\exp^{-\frac{G_K}{\eta_K}t}(0.7R_{fin}\frac{\exp^{\frac{G_K R_{fin}-1.58v_l\eta_K}{\eta_K R_{fin}}t}-\exp^{\frac{G_K R_{fin}-1.58v_l\eta_K}{\eta_K R_{fin}}t_1}\exp^{(t-t_1)\lambda_1^B}}{G_K R_{fin}-1.58\eta_K v_l}+G_K C_1\frac{\exp^{\frac{G_K(t-t_1)}{\eta_K}}-\exp^{(t-t_1)\lambda_1^B}}{\eta_K R_{fin}{}^2(G_K-\eta_K\lambda_1^B)}+\\&\frac{-\exp^{\frac{G_K}{\eta_K}t}+\exp^{\frac{G_K}{\eta_K}t_1}\exp^{(t-t_1)\lambda_1^B}}{G_K-\eta_K\lambda_1^B}+0.7\eta_K\lambda_1^B R_{fin}{}^2\exp^{-\frac{1.58v_l}{R_{fin}}t}\frac{-\exp^{\frac{G_K}{\eta_K}t}+\exp^{(\frac{G_K R_{fin}-1.58v_l\eta_K}{\eta_K R_{fin}}-\lambda_1^B)t_1}\exp^{(\frac{1.58v_l}{R_{fin}}+\lambda_1^B)t}}{(G_K R_{fin}-1.58\eta_K v_l)(1.58\eta_K v_l+R_{fin}(\eta_K\lambda_1^B-G_K))}+\\&\frac{1}{G_H}(0.7\exp^{\frac{G_K}{\eta_K}t}(\exp^{-\frac{1.58v_l}{R_{fin}}t}-\exp^{-\frac{1.58v_l}{R_{fin}}t_1})+\eta_K\lambda_1^B(0.7\exp^{-\frac{1.58v_l}{R_{fin}}t_1}\frac{\exp^{\frac{G_K}{\eta_K}t}-\exp^{(\frac{G_K}{\eta_K}-\lambda_1^B)t_1}\exp^{\lambda_1^B t}}{-G_K+\eta_K\lambda_1^B}+\\&0.7R_{fin}\frac{\exp^{\frac{G_K R_{fin}-1.58v_l\eta_K}{\eta_K R_{fin}}t}-\exp^{\frac{G_K R_{fin}-1.58v_l\eta_K}{\eta_K R_{fin}}t_1}\exp^{(t-t_1)\lambda_1^B}}{-1.58\eta_K v_l-R_{fin}(\eta_K\lambda_1^B-G_K)})))\end{aligned}\quad\text{(A5)}$$

where $C_1=D_1(t_0)+R_{fin}D_2(t_1)$. The displacement is obtained by substituting Eqs. (A5), (51) and (55) into Eq. (35):

$$\begin{aligned}u_{r3}(r,t)&=-\frac{1}{2r}\left\{\begin{aligned}&\frac{1}{G_H}[p_0{}^h\chi(t)-p_{11}(t)]R_{fin}{}^2+\frac{p_0{}^h}{\eta_K}\exp^{-\frac{G_K}{\eta_K}t}\int_0^{t_0}\chi(\tau)R^2(\tau)\exp^{\frac{G_K}{\eta_K}\tau}d\tau\\&+\frac{p_0{}^h}{\eta_K}\exp^{-\frac{G_K}{\eta_K}t}R_{fin}{}^2\int_{t_0}^{t}\chi(\tau)\exp^{\frac{G_K}{\eta_K}\tau}d\tau-\frac{1}{\eta_K}R_{fin}{}^2\exp^{-\frac{G_K}{\eta_K}t}\int_{t_1}^{t}p_{11}(\tau)\exp^{\frac{G_K}{\eta_K}\tau}d\tau\end{aligned}\right\}\\&=-\frac{1}{2r}\left\{\begin{aligned}&\frac{1}{G_H}[p_0{}^h\chi(t)-p_{11}(t)]R_{fin}{}^2+\frac{p_0{}^h}{\eta_K}\exp^{-\frac{G_K}{\eta_K}t}D_1(t_0)\\&+\frac{p_0{}^h}{\eta_K}\exp^{-\frac{G_K}{\eta_K}t}R_{fin}{}^2D_2(t)-\frac{1}{\eta_K}R_{fin}{}^2\exp^{-\frac{G_K}{\eta_K}t}D_3(t)\end{aligned}\right\}\end{aligned}\quad\text{(A6)}$$

where:

$$\begin{aligned}D_3(t)=&\int_{t_1}^{t}p_{11}(\tau)\exp^{\frac{G_K}{\eta_K}\tau}d\tau=e_1p_0{}^h(-\eta_K\frac{\exp^{\frac{G_K}{\eta_K}t}-\exp^{\frac{G_K}{\eta_K}t_1}}{G_K{}^2}-0.7\eta_K\exp^{-\frac{1.58v_l}{R_{fin}}t_1}\frac{\exp^{\frac{G_K}{\eta_K}t}-\exp^{\frac{G_K}{\eta_K}t_1}}{G_KG_H}+\\&C_1\frac{\exp^{\frac{G_K}{\eta_K}(t-t_1)}-1}{G_KR_{fin}{}^2}+0.7\eta_KR_{fin}{}^2\frac{-\exp^{\frac{G_K R_{fin}-1.58v_l\eta_K}{\eta_K R_{fin}}t_1}+\exp^{\frac{G_K R_{fin}-1.58v_l\eta_K}{\eta_K R_{fin}}t}}{(G_KR_{fin}-1.58\eta_Kv_l)^2}+0.7\eta_KR_{fin}\cdot\\&\frac{-\exp^{\frac{G_K R_{fin}-1.58v_l\eta_K}{\eta_K R_{fin}}t_1}+\exp^{\frac{G_K R_{fin}-1.58v_l\eta_K}{\eta_K R_{fin}}t}}{G_H(G_KR_{fin}-1.58\eta_Kv_l)}+\exp^{\frac{G_K-\eta_K\lambda_1^B}{\eta_K}t_1}\frac{\exp^{\lambda_1^Bt}-\exp^{\lambda_1^Bt_1}}{G_K\lambda_1^B}-C_1\frac{\exp^{(t-t_1)\lambda_1^B}-1}{\eta_K\lambda_1^BR_{fin}{}^2}-\\&0.7R_{fin}\exp^{(\frac{G_K R_{fin}-1.58v_l\eta_K}{\eta_K R_{fin}}-\lambda_1^B)t_1}\frac{\exp^{\lambda_1^Bt}-\exp^{\lambda_1^Bt_1}}{(G_KR_{fin}-1.58\eta_Kv_l)\lambda_1^B}-C_1\frac{\exp^{(t-t_1)\lambda_1^B}-1}{R_{fin}{}^2(G_K-\eta_K\lambda_1^B)}+C_1\eta_K\lambda_1^B\frac{\exp^{\frac{G_K}{\eta_K}(t-t_1)}-1}{G_KR_{fin}{}^2(G_K-\eta_K\lambda_1^B)}+\end{aligned}$$

$$\eta_K \exp^{\frac{G_K-\eta_K\lambda_1^B}{\eta_K}t_1}\frac{\exp^{\lambda_1^B t}-\exp^{\lambda_1^B t_1}}{G_K(G_K-\eta_K\lambda_1^B)}-\eta_K{}^2\lambda_1^B\frac{\exp^{\frac{G_K}{\eta_K}t}-\exp^{\frac{G_K}{\eta_K}t_1}}{G_K{}^2(G_K-\eta_K\lambda_1^B)}+0.7\eta_K\exp^{(\frac{G_K R_{fin}-1.58v_l\eta_K}{\eta_K R_{fin}}-\lambda_1^B)t_1}\frac{\exp^{\lambda_1^B t}-\exp^{\lambda_1^B t_1}}{G_H(G_K-\eta_K\lambda_1^B)}-$$

$$0.7\eta_K{}^2\lambda_1^B\exp^{-\frac{1.58v_l}{R_{fin}}t_1}\frac{\exp^{\frac{G_K}{\eta_K}t}-\exp^{\frac{G_K}{\eta_K}t_1}}{G_H G_K(G_K-\eta_K\lambda_1^B)}+0.7\eta_K R_{fin}\exp^{(\frac{G_K R_{fin}-1.58v_l\eta_K}{\eta_K R_{fin}}-\lambda_1^B)t_1}\frac{\exp^{\lambda_1^B t}-\exp^{\lambda_1^B t_1}}{G_H(1.58\eta_K v_l+R_{fin}(\eta_K\lambda_1^B-G_K))}+$$

$$0.7\eta_K R_{fin}{}^2\exp^{(\frac{G_K R_{fin}-1.58v_l\eta_K}{\eta_K R_{fin}}-\lambda_1^B)t_1}\frac{\exp^{\lambda_1^B t}-\exp^{\lambda_1^B t_1}}{(G_K R_{fin}-1.58\eta_K v_l)(1.58\eta_K v_l+R_{fin}(\eta_K\lambda_1^B-G_K))}-$$

$$0.7\eta_K{}^2R_{fin}{}^3\lambda_1^B\cdot\frac{-\exp^{\frac{G_K R_{fin}-1.58v_l\eta_K}{\eta_K R_{fin}}t_1}+\exp^{\frac{G_K R_{fin}-1.58v_l\eta_K}{\eta_K R_{fin}}t}}{(G_K R_{fin}-1.58\eta_K v_l)^2(1.58\eta_K v_l+R_{fin}(\eta_K\lambda_1^B-G_K))}-$$

$$0.7\eta_K{}^2R_{fin}{}^2\lambda_1^B\frac{-\exp^{\frac{G_K R_{fin}-1.58v_l\eta_K}{\eta_K R_{fin}}t_1}+\exp^{\frac{G_K R_{fin}-1.58v_l\eta_K}{\eta_K R_{fin}}t}}{G_H(G_K R_{fin}-1.58\eta_K v_l)(1.58\eta_K v_l+R_{fin}(\eta_K\lambda_1^B-G_K))})$$

(A7)

When $t_2 \le t < t_3$, i.e. during the second liner stage, the support pressure acting on the rock is obtained by substituting Eq. (44) into Eq.(41):

$$p_{12}(t)=-C_4+C_3\exp^{-\frac{G_K}{\eta_K}t}\exp^{(t-t_2)\lambda_2^B}-C_4\eta_K\lambda_2^B\frac{1-\exp^{-(\frac{G_K}{\eta_K}-\lambda_2^B)(t-t_2)}}{G_K-\eta_K\lambda_2^B}+e_2p_0{}^h\exp^{-\frac{G_K}{\eta_K}t}(0.7R_{fin}\cdot$$

$$\frac{\exp^{\frac{G_K R_{fin}-1.58v_l\eta_K}{\eta_K R_{fin}}t}-\exp^{\frac{G_K R_{fin}-1.58v_l\eta_K}{\eta_K R_{fin}}t_2}\exp^{(t-t_2)\lambda_2^B}}{G_K R_{fin}-1.58\eta_K v_l}-C_1\exp^{-\frac{G_K}{\eta_K}t_1}\frac{-G_K\exp^{\frac{G_K}{\eta_K}t}+\eta_K\lambda_2^B\exp^{\lambda_2^B t}\exp^{(\frac{G_K}{\eta_K}-\lambda_2^B)t_2}}{\eta_K R_{fin}{}^2(G_K-\eta_K\lambda_2^B)}$$

$$+\frac{-\exp^{\frac{G_K}{\eta_K}t}+\exp^{\frac{G_K}{\eta_K}t_2}\exp^{(t-t_2)\lambda_2^B}}{G_K-\eta_K\lambda_2^B}+0.7\eta_K\lambda_2^B R_{fin}{}^2\exp^{-\frac{1.58v_l}{R_{fin}}t}\frac{-\exp^{\frac{G_K}{\eta_K}t}+\exp^{(\frac{G_K R_{fin}-1.58v_l\eta_K}{\eta_K R_{fin}}-\lambda_2^B)t_2}\exp^{(\frac{1.58v_l}{R_{fin}}+\lambda_2^B)t}}{(G_K R_{fin}-1.58\eta_K v_l)(1.58\eta_K v_l+R_{fin}(\eta_K\lambda_2^B-G_K))}+$$

$$\frac{1}{G_H}(0.7\exp^{\frac{G_K}{\eta_K}t}(\exp^{-\frac{1.58v_l}{R_{fin}}t}-\exp^{-\frac{1.58v_l}{R_{fin}}t_1})+\eta_K\lambda_2^B(0.7\exp^{-\frac{1.58v_l}{R_{fin}}t_1}\frac{\exp^{\frac{G_K}{\eta_K}t}-\exp^{(\frac{G_K}{\eta_K}-\lambda_2^B)t_2}\exp^{\lambda_2^B t}}{-G_K+\eta_K\lambda_2^B}+$$

$$0.7R_{fin}\frac{\exp^{\frac{G_K R_{fin}-1.58v_l\eta_K}{\eta_K R_{fin}}t}-\exp^{\frac{G_K R_{fin}-1.58v_l\eta_K}{\eta_K R_{fin}}t_2}\exp^{(t-t_2)\lambda_2^B}}{-1.58\eta_K v_l-R_{fin}(\eta_K\lambda_2^B-G_K)})))$$

(A8)

where $C_2=D_1(t_0)+R_{fin}D_2(t_2)$, $C_3=-\frac{p_0{}^h e_2}{\eta_K R_{fin}{}^2}C_2+\lambda_2^B D_3(t_2)$, $C_4=\frac{2e_2a_{01}a_{10}}{a_{11}R_1}p_{11}(t_2)$. The displacement is obtained by substituting Eqs.(A8), (51) and (55) into Eq. (35) so we get:

$$u_{r4}(r,t)=-\frac{1}{2r}\left\{\begin{array}{l}\frac{1}{G_H}[p_0{}^h\chi(t)-p_{12}(t)]R_{fin}{}^2+\frac{p_0{}^h}{\eta_K}\exp^{-\frac{G_K}{\eta_K}t}\int_0^{t_0}\chi(\tau)R^2(\tau)\exp^{\frac{G_K}{\eta_K}\tau}d\tau+\frac{p_0{}^h}{\eta_K}\exp^{-\frac{G_K}{\eta_K}t}R_{fin}{}^2\cdot\\ \int_{t_0}^{t}\chi(\tau)\exp^{\frac{G_K}{\eta_K}\tau}d\tau-\frac{1}{\eta_K}R_{fin}{}^2\exp^{-\frac{G_K}{\eta_K}t}\int_{t_1}^{t_2}p_{11}(\tau)\exp^{\frac{G_K}{\eta_K}\tau}d\tau-\frac{1}{\eta_K}R_{fin}{}^2\exp^{-\frac{G_K}{\eta_K}t}\int_{t_2}^{t}p_{12}(\tau)\exp^{\frac{G_K}{\eta_K}\tau}d\tau\end{array}\right\}$$

$$
=-\frac{1}{2r}\left\{\begin{aligned}&\frac{1}{G_H}[p_0{}^h\chi(t)-p_{12}(t)]R_{fin}{}^2+\frac{p_0{}^h}{\eta_K}\exp^{-\frac{G_K}{\eta_K}t}D_1(t_1)+\frac{p_0{}^h}{\eta_K}\exp^{-\frac{G_K}{\eta_K}t}R_{fin}{}^2D_2(t)\\&-\frac{1}{\eta_K}R_{fin}{}^2\exp^{-\frac{G_K}{\eta_K}t}D_3(t_2)-\frac{1}{\eta_K}R_{fin}{}^2\exp^{-\frac{G_K}{\eta_K}t}D_4(t)\end{aligned}\right\} \tag{A9}
$$

where:

$$
\begin{aligned}
D_4(t)&=\int_{t_2}^{t}p_{12}(\tau)\exp^{\frac{G_K}{\eta_K}\tau}d\tau\\
&=-\frac{C_4\eta_K}{G_K}(\exp^{\frac{G_K}{\eta_K}t}-\exp^{\frac{G_K}{\eta_K}t_2})+\frac{C_3}{\lambda_2^B}(-1+\exp^{(t-t_2)\lambda_2^B})+C_4\eta_K\exp^{\frac{G_K-\eta_K\lambda_2^B}{\eta_K}t_2}\frac{\exp^{\lambda_2^B t}-\exp^{\lambda_2^B t_2}}{G_K-\eta_K\lambda_2^B}-C_4\eta_K{}^2\lambda_2^B\frac{\exp^{\frac{G_K}{\eta_K}t}-\exp^{\frac{G_K}{\eta_K}t_2}}{G_K(G_K-\eta_K\lambda_2^B)}\\
&+e_2p_0{}^h(-\eta_K\frac{\exp^{\frac{G_K}{\eta_K}t}-\exp^{\frac{G_K}{\eta_K}t_2}}{G_K{}^2}-0.7\eta_K\exp^{-\frac{1.58v_l}{R_{fin}}t_1}\frac{\exp^{\frac{G_K}{\eta_K}t}-\exp^{\frac{G_K}{\eta_K}t_2}}{G_KG_H}+C_1\frac{\exp^{\frac{G_K}{\eta_K}(t-t_1)}-\exp^{\frac{G_K}{\eta_K}(t_2-t_1)}}{G_KR_{fin}{}^2}+\\
&+0.7\eta_KR_{fin}{}^2\frac{-\exp^{\frac{G_KR_{fin}-1.58v_l\eta_K}{\eta_KR_{fin}}t_2}+\exp^{\frac{G_KR_{fin}-1.58v_l\eta_K}{\eta_KR_{fin}}t}}{(G_KR_{fin}-1.58\eta_Kv_l)^2}+0.7\eta_KR_{fin}\frac{-\exp^{\frac{G_KR_{fin}-1.58v_l\eta_K}{\eta_KR_{fin}}t_2}+\exp^{\frac{G_KR_{fin}-1.58v_l\eta_K}{\eta_KR_{fin}}t}}{G_H(G_KR_{fin}-1.58\eta_Kv_l)}+\exp^{\frac{G_K-\eta_K\lambda_2^B}{\eta_K}t_2}\cdot\\
&\cdot\frac{\exp^{\lambda_2^Bt}-\exp^{\lambda_2^Bt_2}}{G_K\lambda_2^B}-0.7R_{fin}\exp^{(\frac{G_KR_{fin}-1.58v_l\eta_K}{\eta_KR_{fin}}-\lambda_2^B)t_2}\frac{\exp^{\lambda_2^Bt}-\exp^{\lambda_2^Bt_2}}{(G_KR_{fin}-1.58\eta_Kv_l)\lambda_2^B}-C_1\exp^{\frac{G_K}{\eta_K}(t_2-t_1)}\frac{\exp^{(t-t_1)\lambda_2^B}-1}{R_{fin}{}^2(G_K-\eta_K\lambda_2^B)}+\\
&+C_1\eta_K\lambda_2^B\frac{\exp^{\frac{G_K}{\eta_K}(t-t_1)}-\exp^{\frac{G_K}{\eta_K}(t_2-t_1)}}{G_KR_{fin}{}^2(G_K-\eta_K\lambda_2^B)}+\eta_K\exp^{\frac{G_K-\eta_K\lambda_2^B}{\eta_K}t_2}\frac{\exp^{\lambda_2^Bt}-\exp^{\lambda_2^Bt_2}}{G_K(G_K-\eta_K\lambda_2^B)}-\eta_K{}^2\lambda_2^B\frac{\exp^{\frac{G_K}{\eta_K}t}-\exp^{\frac{G_K}{\eta_K}t_2}}{G_K{}^2(G_K-\eta_K\lambda_2^B)}+\\
&+0.7\eta_K\exp^{\frac{G_KR_{fin}t_2-1.58v_l\eta_Kt_1}{\eta_KR_{fin}}-\lambda_2^Bt_2}\frac{\exp^{\lambda_2^Bt}-\exp^{\lambda_2^Bt_2}}{G_H(G_K-\eta_K\lambda_2^B)}-0.7\eta_K{}^2\lambda_2^B\exp^{-\frac{1.58v_l}{R_{fin}}t_1}\frac{\exp^{\frac{G_K}{\eta_K}t}-\exp^{\frac{G_K}{\eta_K}t_2}}{G_HG_K(G_K-\eta_K\lambda_2^B)}+\\
&+0.7\eta_KR_{fin}\exp^{(\frac{G_KR_{fin}-1.58v_l\eta_K}{\eta_KR_{fin}}-\lambda_2^B)t_2}\frac{\exp^{\lambda_2^Bt}-\exp^{\lambda_2^Bt_2}}{G_H(1.58\eta_Kv_l+R_{fin}(\eta_K\lambda_2^B-G_K))}+\\
&+0.7\eta_KR_{fin}{}^2\exp^{(\frac{G_KR_{fin}-1.58v_l\eta_K}{\eta_KR_{fin}}-\lambda_2^B)t_2}\frac{\exp^{\lambda_2^Bt}-\exp^{\lambda_2^Bt_2}}{(G_KR_{fin}-1.58\eta_Kv_l)(1.58\eta_Kv_l+R_{fin}(\eta_K\lambda_2^B-G_K))}-\\
&+0.7\eta_K{}^2R_{fin}{}^3\lambda_2^B\cdot\frac{-\exp^{\frac{G_KR_{fin}-1.58v_l\eta_K}{\eta_KR_{fin}}t_2}+\exp^{\frac{G_KR_{fin}-1.58v_l\eta_K}{\eta_KR_{fin}}t}}{(G_KR_{fin}-1.58\eta_Kv_l)^2(1.58\eta_Kv_l+R_{fin}(\eta_K\lambda_2^B-G_K))}-\\
&+0.7\eta_K{}^2R_{fin}{}^2\lambda_2^B\frac{-\exp^{\frac{G_KR_{fin}-1.58v_l\eta_K}{\eta_KR_{fin}}t_2}+\exp^{\frac{G_KR_{fin}-1.58v_l\eta_K}{\eta_KR_{fin}}t}}{G_H(G_KR_{fin}-1.58\eta_Kv_l)(1.58\eta_Kv_l+R_{fin}(\eta_K\lambda_2^B-G_K))})
\end{aligned} \tag{A10}
$$

When $t\ge t_3$, i.e. during the third liner stage, the displacement is obtained by substituting Eqs. (51) and (55) into Eq. (35):

$$u_{r5}(r,t) = -\frac{1}{2r}\left\{\begin{array}{l} \frac{1}{G_H}[p_0{}^h\chi(t) - p_{13}(t)]R_{fin}{}^2 + \frac{p_0{}^h}{\eta_K}\exp^{-\frac{G_K}{\eta_K}t}\int_0^{t_0}\chi(\tau)R^2(\tau)\exp^{\frac{G_K}{\eta_K}\tau}d\tau + \frac{p_0{}^h}{\eta_K}\exp^{-\frac{G_K}{\eta_K}t}R_{fin}{}^2\cdot \\ \int_{t_0}^{t}\chi(\tau)\exp^{\frac{G_K}{\eta_K}\tau}d\tau - \frac{1}{\eta_K}R_{fin}{}^2\exp^{-\frac{G_K}{\eta_K}t}\int_{t_1}^{t_2}p_{11}(\tau)\exp^{\frac{G_K}{\eta_K}\tau}d\tau - \frac{1}{\eta_K}R_{fin}{}^2\exp^{-\frac{G_K}{\eta_K}t}\int_{t_2}^{t_3}p_{12}(\tau)\exp^{\frac{G_K}{\eta_K}\tau}d\tau \\ -\frac{1}{\eta_K}R_{fin}{}^2\exp^{-\frac{G_K}{\eta_K}t}\int_{t_3}^{t}p_{13}(\tau)\exp^{\frac{G_K}{\eta_K}\tau}d\tau \end{array}\right\}$$

$$= -\frac{1}{2r}\left\{\begin{array}{l} \frac{1}{G_H}[p_0{}^h\chi(t) - p_{13}(t)]R_{fin}{}^2 + \frac{p_0{}^h}{\eta_K}\exp^{-\frac{G_K}{\eta_K}t}D_1(t_0) + \frac{p_0{}^h}{\eta_K}\exp^{-\frac{G_K}{\eta_K}t}R_{fin}{}^2 D_2(t) \\ -\frac{1}{\eta_K}R_{fin}{}^2\exp^{-\frac{G_K}{\eta_K}t}D_3(t_2) - \frac{1}{\eta_K}R_{fin}{}^2\exp^{-\frac{G_K}{\eta_K}t}D_4(t_3) - \frac{1}{\eta_K}R_{fin}{}^2\exp^{-\frac{G_K}{\eta_K}t}D_5(t) \end{array}\right\} \qquad \text{(A11)}$$

The analytical expressions for $p_{13}(t)$ and $D_5(t)$ are obtained by replacing the coefficients in the expressions of $p_{12}(t)$ and $D_4(t)$ respectively (see Eqs. (A8), (A10)) as follows:

$C_3 \to C_6$; $C_4 \to C_7$; $t_2 \to t_3$; $e_2 \to e_3$; $\lambda_2^B \to \lambda_3^B$;

with:

$$C_5 = D_1(t_0) + R_{fin}D_2(t_3),\quad C_6 = -\frac{p_0{}^h e_2}{\eta_K R_{fin}{}^2}C_5 + \lambda_3^B[D_3(t_2) + D_4(t_3)],$$

$$C_7 = \frac{2e_3 a_{01}}{R_1(a_{11}a_{22} - a_{21}a_{12})}[a_{10}a_{22}p_{11}(t_2) - a_{21}a_{12}p_{22}(t_3)],\quad p_{22}(t) = \frac{1}{a_{11}}[a_{10}p_{11}(t_2) - a_{10}p_{12}(t)].$$

References

1 Carranza-Tores C, Fairhurst C. The elastoplastic response of underground excavations in rock masses that satisfy the Hoek-Brown failure criterion. Int. J. Rock Mech. Min. Sci. Geomech. Abst. 1999; 36: 777-809.

2 Malan DF. Simulating the time-dependent behaviour of excavations in hard rock. Rock Mech. Rock Engrg. 2002; 35(4): 225-254.

3 Tonon F. Sequential excavation, NATM and ADECO: What they have in common and how they differ. Tunnelling & Underground Space Technology 2010; 25: 245-265.

4 Sharifzadeh M, Daraei R, Broojerdi M. Design of sequential excavation tunneling in weak rocks through findings obtained from displacements based back analysis. Tunnelling & Underground Space Technology 2012; 28: 10-17.

5 Xu L, Huang HW. Time effects in rock-support interaction: a case study in the construction of two road tunnels. Int. J. Rock Mech. Min. Sci. 2004; 41(suppl. 1): 888-893.

6 Jaeger JC, Cook NGW, Zimmerman RW. Fundamentals of rock mechanics, 4th edition. USA: Blackwell; 2007.

7 Pan YW, Dong JJ. Time dependent tunnel convergence II. Advance rate and tunnel support interaction. Int. J. Rock Mech. Min. Sci. 1991; 28: 477-488.

8 Gnirk PF, Johnson RE. The deformational behavior of a circular mine shaft situated in a viscoelastic medium under hydrostatic stress. In: Proceeding of 6th Symposium Rock Mechanics. University of Missouri Rolla; 28-30October 1964. p. 231-259.

9 Ladanyi B, Gill DE. Tunnel lining design in creeping rocks. In: Proceedings of ISRM Symposium on Design and Performance of Underground Excavations. Cambridge; 3-6 September 1984. p. 37-44.

10 Brady B, Brown E. Rock mechanics for underground mining. London: George Allen & Unwin; 1985.

11 Katushi Miura, Hiroshi Yagi, Hiromichi Shiroma, Kazuya Takekuni. Study on design and construction method for the New Tomei-Meishin expressway tunnels. Tunnelling & Underground Space Technology 2003; 18: 271-281.

12 Tetsuo Ito, Wataru Akagi, Hiromichi Shiroma, Akitomo Nakanishi, Shogo Kunimura. Estimation of natural ground behavior ahead of face by measuring deformation which utilized

TBM drift tunnel. Tunnelling & Underground Space Technology 2004; 19: 527-528.
13 Katsushi Miura. Design and construction of mountain tunnels in Japan. Tunnelling & Underground Space Technology 2003; 18: 115-126.
14 Lee EH. Stress analysis in viscoelastic bodies. Quarterly of Applied Mathematics 1955; 13(2):183-190.
15 Christensen RM. Theory of viscoelasticity: An introduction 2nd ed. New York: Academic Press; 1982.
16 Gurtin ME, Sternberg E. On the linear theory of viscoelasticity. Arch Ration Mech Anal 1962; 11: 2914-356.
17 Savin GN. Stress concentration around holes. London: Pergamon Press; 1961.
18 Peck RB, Hendron AJ, Mohraz B. State of the art of soft ground tunneling. In: Proceedings of the Rapid Excavation Tunneling Conference Volume 1, Chicago; June 1972. p. 259-286.
19 Einstein HH, Schwartz CW. Simplified analysis for tunnel supports. Journal of Geotechnical Engineering Division (ASCE) 1979; GT4(April): 499-518.
20 Sulem J, Panet M, Guenot A. An analytical solution for time-dependent displacements in circular tunnel. Int. J. Rock Mech. Min. Sci. Geomech. Abst. 1987; 24(3): 155-164.
21 Nomikos P, Rahmannejad R, Sofianos A. Supported axisymmetric tunnels within linear viscoelastic Burgers rocks. Rock Mech. Rock Engrg. 2011; 44: 553-564.
22 Mason DP, Stacey TR. Support to rock excavations provided by sprayed liners. Int. J. Rock Mech. Min. Sci. 2008; 45: 773-788.
23 Mason DP, Abelman H. Support provided to excavations by a system of two liners. Int. J. Rock Mech. Min. Sci. 2009; 46: 1197-1205.
24 Dai HL, Wang X, Xie GX, Wang XY. Theoretical model and solution for the rheological problem of anchor-grouting a soft rock tunnel. Int. J. of Pressure Vessels and Piping 2004; 81:739-748.
25 Thompson AG, Villaescusa E, Windsor CR. Ground support terminology and classification: un update. Geotechnical and Geological Engineering 2012; 30: 553–580.
26 Wang HN, Li Y, Ni Q, Utili S, Jiang MJ, Liu F. Analytical solutions for the construction of deeply buried circular tunnels with two liners in rheological rock. Rock Mech. Rock Engrg. 2013; 46(6): 1481-1498.

27 Schuerch R, Anagnostou G. The applicability of the ground response curve to tunnelling problems that violate rotational symmetry. Rock Mech. Rock Engrg. 2012; 45(1): 1-10.

28 Hoek E, Carranza-Torres C, Diederichs MS, Corkum B. Integration of geotechnical and structural design in tunnelling. In: Proceedings university of minnesota 56th annual geotechnical engineering conference. Minneapolis; 29 February 2008. p1-53.

29 Wang HN, Nie GH. Analytical expressions for stress and displacement fields in viscoelastic axisymmetric plane problem involving time-dependent boundary regions. Acta Mechanica 2010; 210: 315-330.

30 Chambers LG. Integral Equations: A short course. London: International Textbooks Co Ltd; 1976.

31 Jiao LL, Song L, Wang XZ, Adoko AC. Improvement of the U shaped steel sets for supporting the roadways in loose thick coal seam. International Journal of rock mechanics and mining sciences 2013; 60: 19-25.

32 Carranza-Torres C, Diederichs M. Mechanical analysis of circular liners with particular reference to composite supports. For example, liners consisting of shotcrete and steel sets. Tunnelling and Underground space technology 2009; 24: 506-532.

33 Liu BG, Du XD. Visco-elastic analysis on interaction between supporting structure and surrounding rocks of circle tunnel. Chinese Journal of Rock Mechanics and Engineering 2004; 23(4): 561-564 (in Chinese).

34 Panet M, Guenot A. Analysis of convergence behind the face of a tunnel. In: Proceedings of the 3rd International Symposium. Brighton; 7-11 June 1982. p. 197-204.

35 Li XH, Li DX, Jin XG, Gu YL. Discussion on influence of initial support to stability and deformation of surrounding rock mass in soft rock tunnel. Rock and Soil Mechanics 2005; 26(8):1207-1210 (in Chinese).

Legends

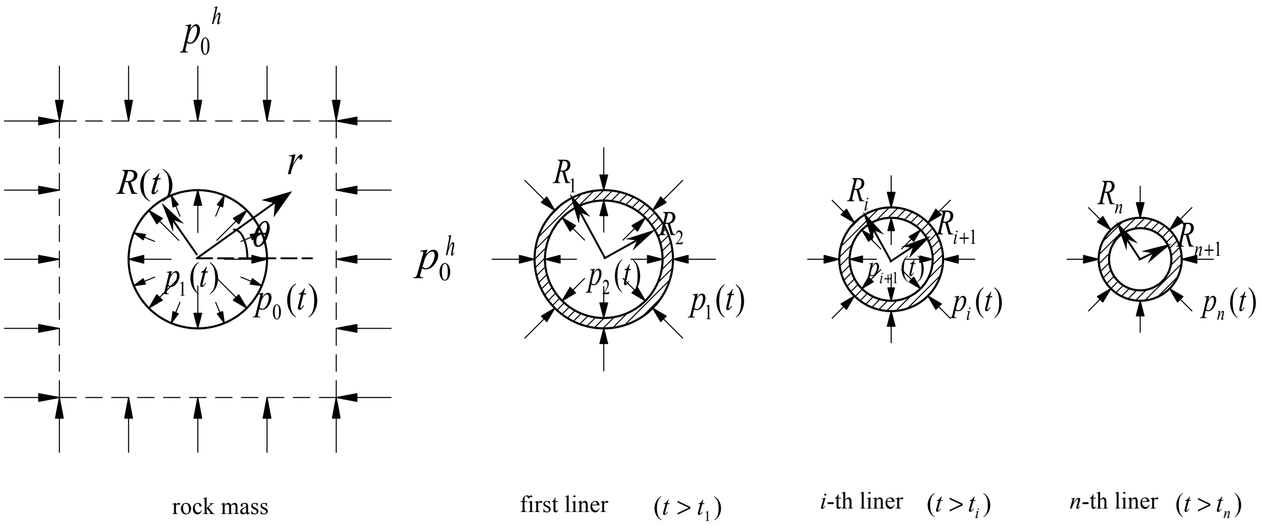

Figure 1 Illustration of the radii of the liners and of the support pressures.

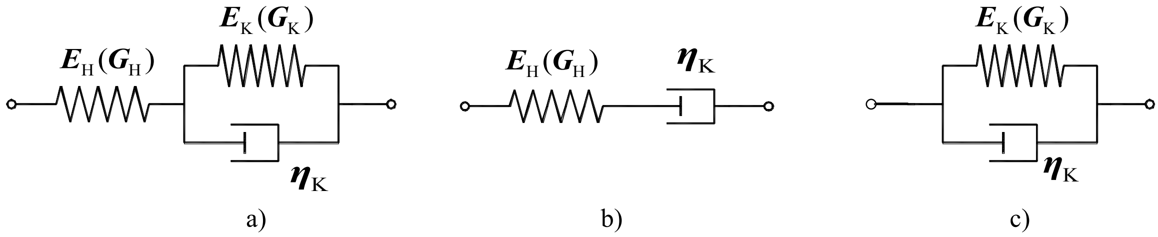

Figure 2 a) Generalised Kelvin model. b) for G_K=0, the Maxwell model is obtained; c)for $G_H \to \infty$, the Kelvin model is obtained.

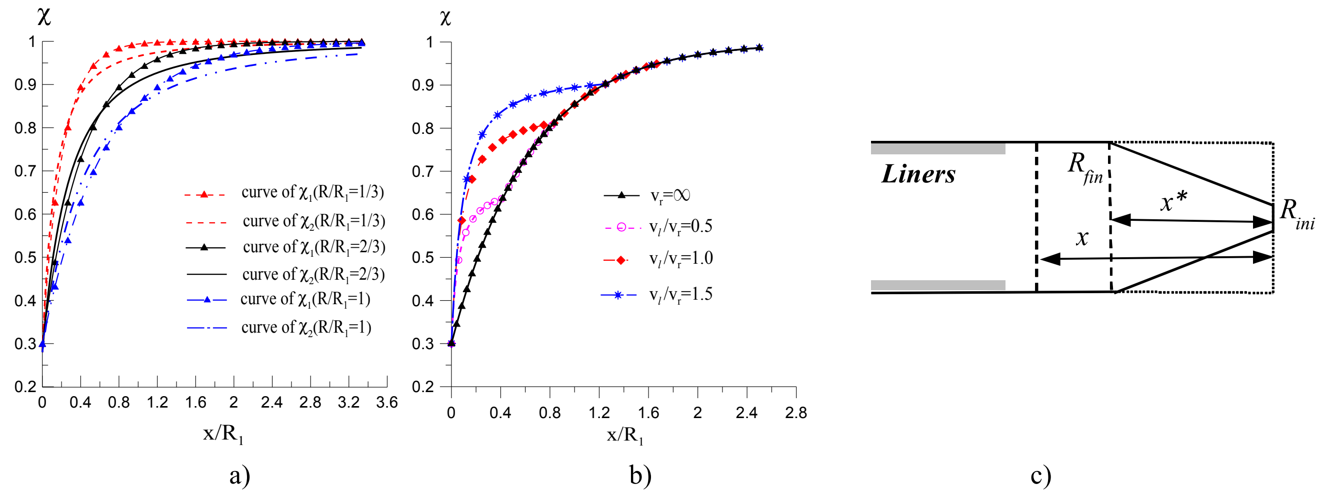

Figure 3 Parameter accounting for the tunnel face effect: a) curves obtained from expressions proposed by Liu[33], χ_1, and Panet and Guenot [34], χ_2, against the distance of the considered section from the tunnel face normalized by the final radius of the section; b) curves obtained from the adopted expression [33] calculated for different ratios of excavation speed against the normalized distance; c) sketch showing the approximation introduced in the calculation of χ: the dotted line indicates the excavated volume assumed in the calculation of Panet and Guenot [34] whilst the solid line indicates the real excavated volume.

Table 1 Geometrical and mechanical parameters for the liners in dimensionless form.

Parameters	$\frac{G_1^L}{G_H}$	$\frac{G_2^L}{G_H}$	$\frac{G_3^L}{G_H}$	ν_1^L	ν_2^L	ν_3^L	$\frac{R_2 - R_1}{R_1}$	$\frac{R_3 - R_2}{R_1}$	$\frac{R_4 - R_3}{R_1}$	$\frac{t_1}{t_0}$	$\frac{t_2}{t_0}$	$\frac{t_3}{t_0}$
Value	16	16	20	0.2	0.2	0.2	$\frac{1}{120}$	$\frac{1}{60}$	$\frac{1}{30}$	1	$\frac{7}{5}$	$\frac{11}{5}$

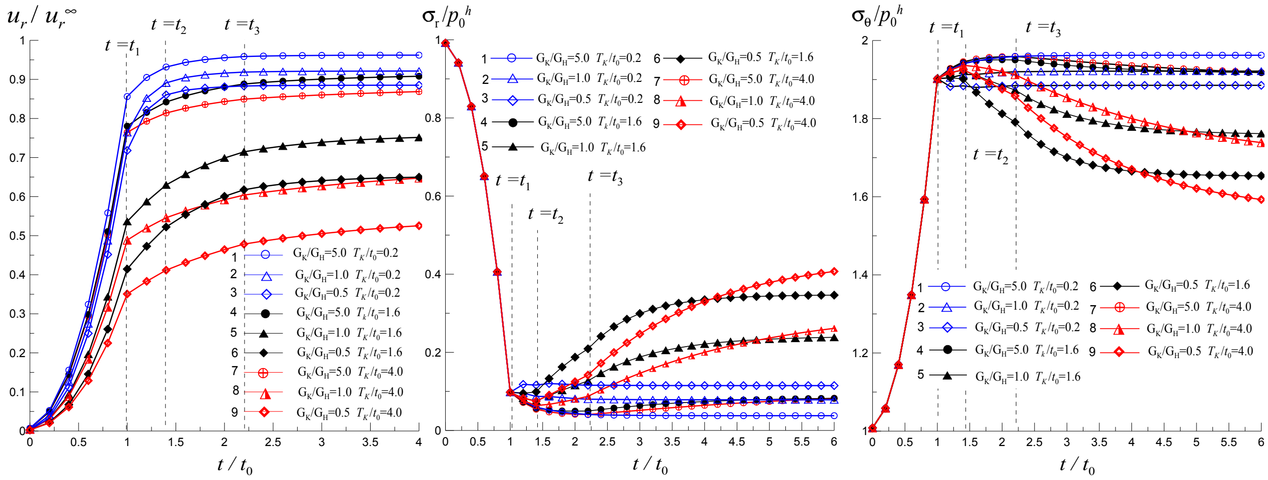

a) b) c)

Figure 4. Generalized Kelvin model; curves obtained for various values of T_K/t_0 and G_K/G_H: a) normalized radial convergence versus time normalized by the excavation time t_0; b) normalized radial stress versus normalized time; c) normalized hoop stress versus normalized time. Note that at the end of the excavation process, $t/t_0=1$, all the curves exhibit a kink point.

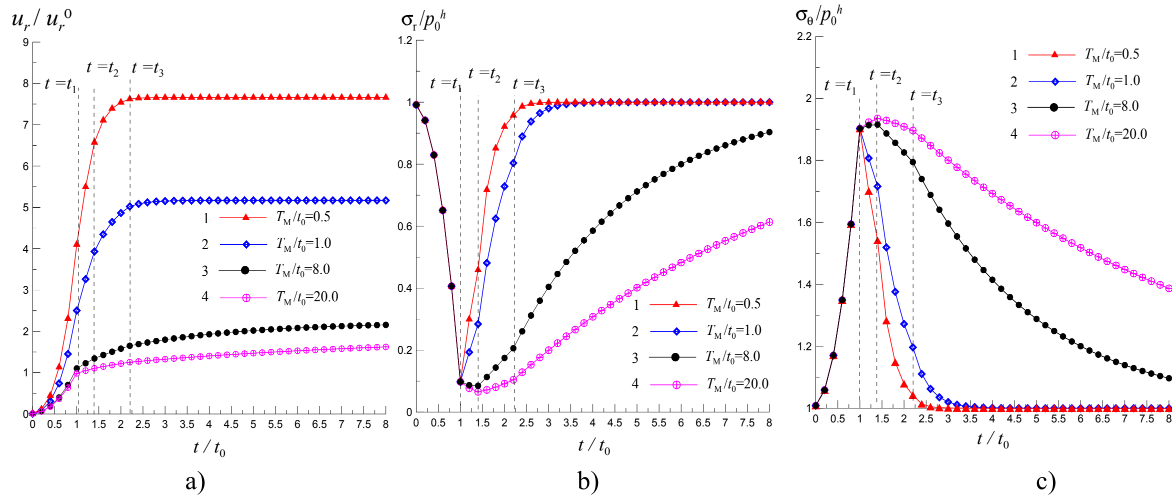

Figure 5. Maxwell model, curves obtained for various values of T_M/t_0 and $G_K = 0$: a) Normalized radial convergence versus time normalized by the excavation time, t_0; b) normalized radial stress versus normalized time; c) normalized hoop stress versus normalized time. Note that at the end of the excavation process, $t/t_0 = 1$, all the curves exhibit a kink point.

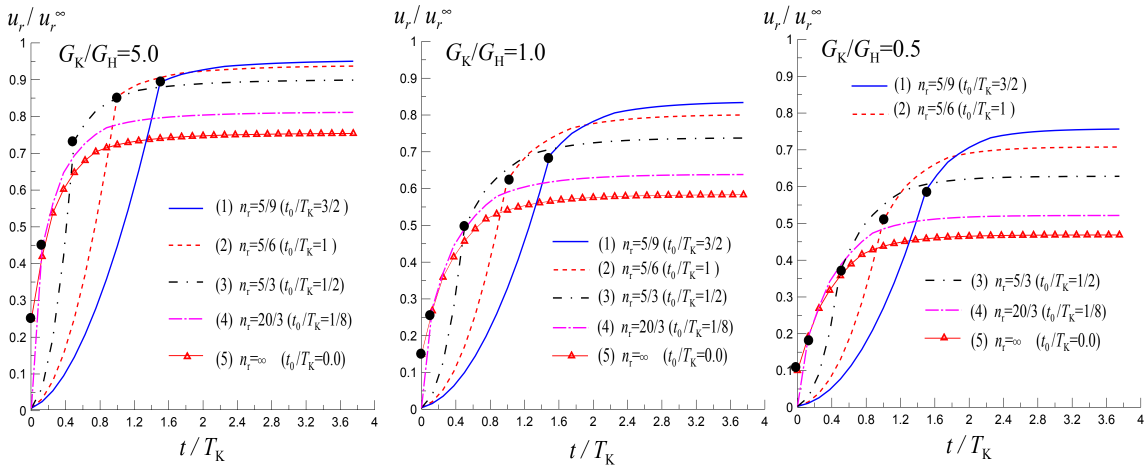

a) b) c)

Figure 6. Generalized Kelvin model: normalized radial convergence versus normalized time for various excavation rates. The '•' symbol denotes the end of the excavation.

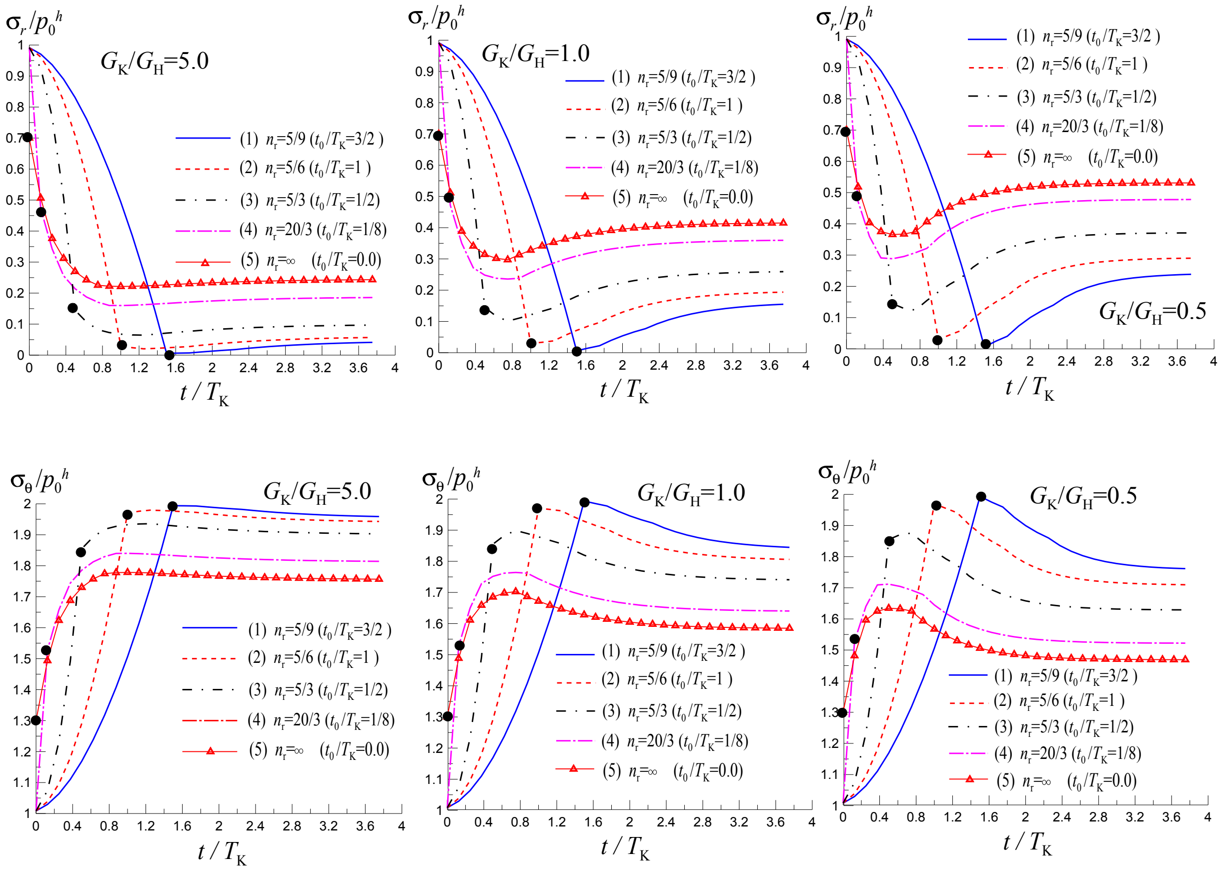

Figure 7. Generalized Kelvin model: normalized stresses at the interface between rock and the first liner $r = R_1$ versus normalized time for various excavation rates. The '●' symbol denotes the end of the excavation.

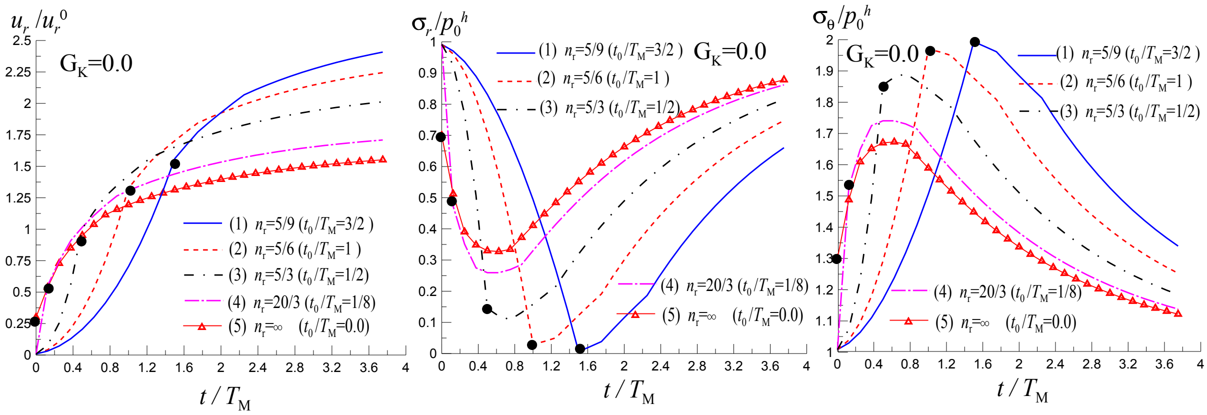

a) b) c)

Figure 8. Maxwell model: a) normalized radial convergence versus normalized time for various excavation rates. b) normalized radial stress and c) normalized hoop stress calculated at the interface between rock and the first liner $r = R_1$ versus normalized time for various excavation rates. The '•' symbol denotes the end of the excavation.

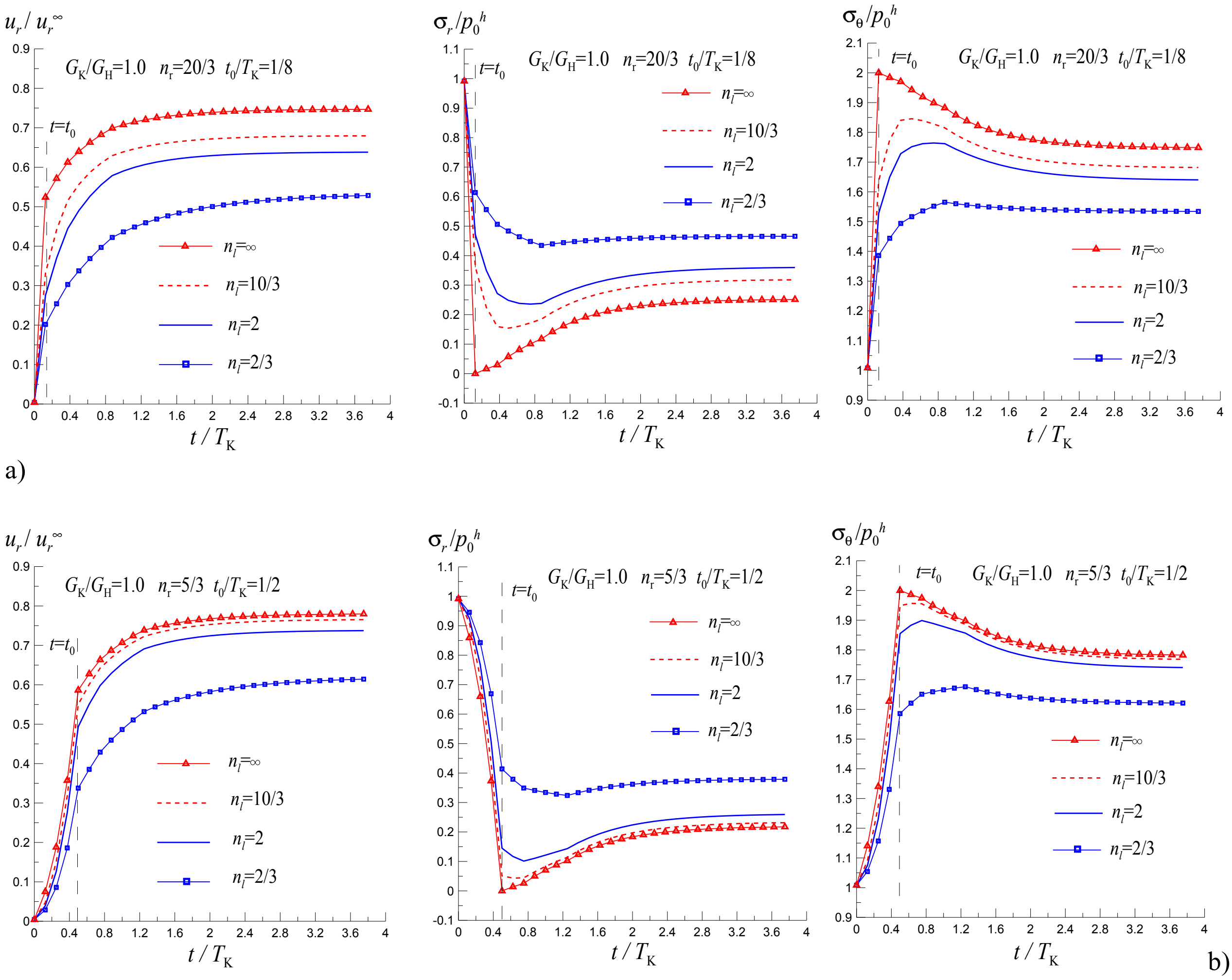

Figure 9. Influence of tunnel advancement for a fast ((a) n_r=20/3) and low ((b) n_r=5/3) cross-section excavation rate. The influence on stresses and displacement is more significant for higher cross section excavation rate.

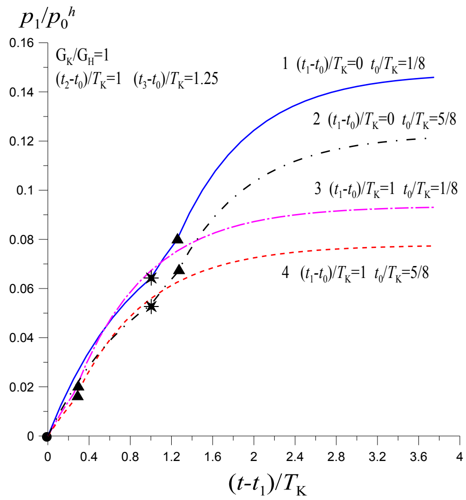

Figure 10. Supporting pressure against time for different installation times. The symbols '●' , '⁎' and '▲' represent the installation times of the first, second and third liners respectively.

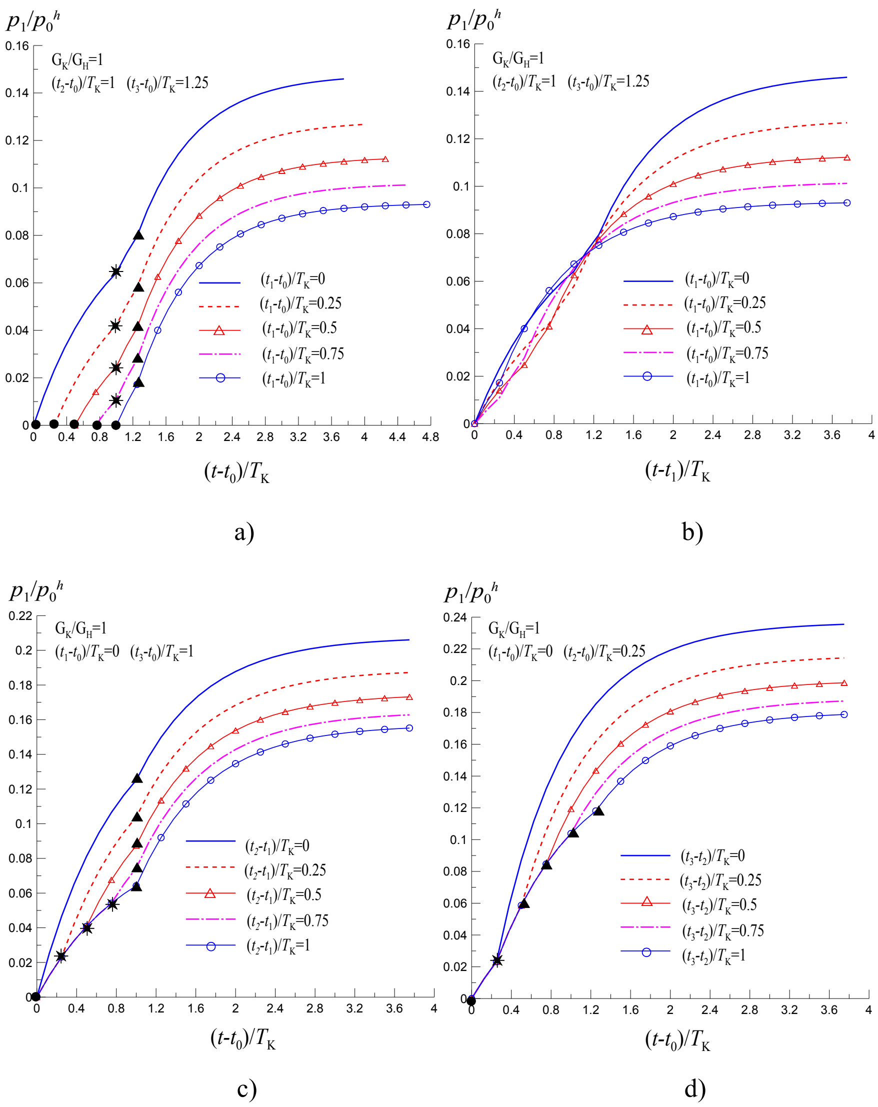

Figure 11. Normalized supporting pressure p_1 against normalized time for different installation times. The symbols '●' , '✳' and '▲' represent the installation times of the first, second and third liners respectively. a) supporting pressure p_1 versus time interval since the end time of excavation for different first liner installation times. b) supporting pressure p_1 versus time interval since the installation of the first liner for different first liner installation times. c) and d) supporting pressure p_1 versus time interval since the end time of excavation for different second and third liner installation times, respectively.

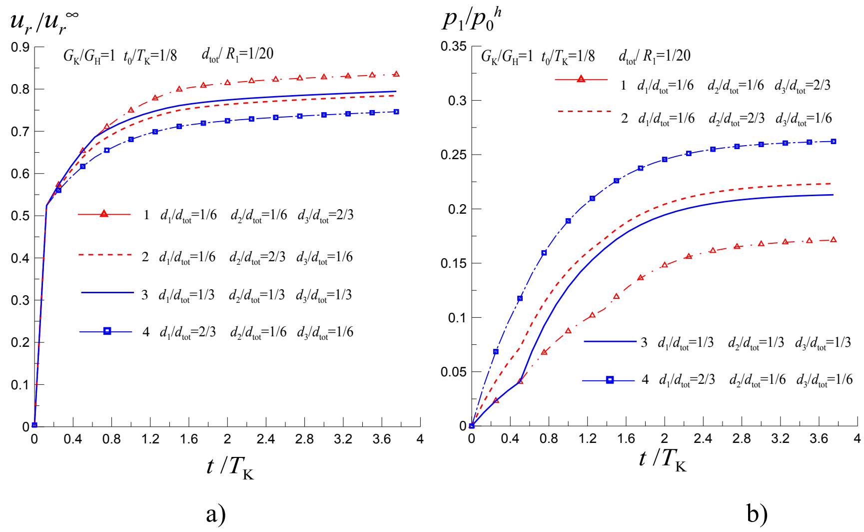

Figure 12. Influence of the liner thicknesses: a) normalized radial convergence versus normalized time for various liner thicknesses; b) support pressure versus normalized time.

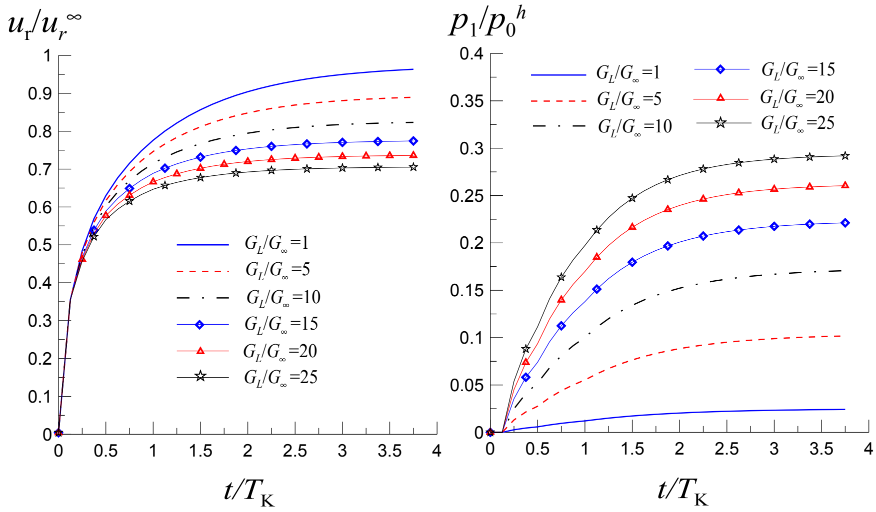

a) b)

Figure 13. Influence of the modular ratio G_L / G_∞ between liners and rock: a) normalized radial convergence versus normalized time; b) normalized support pressure versus time.

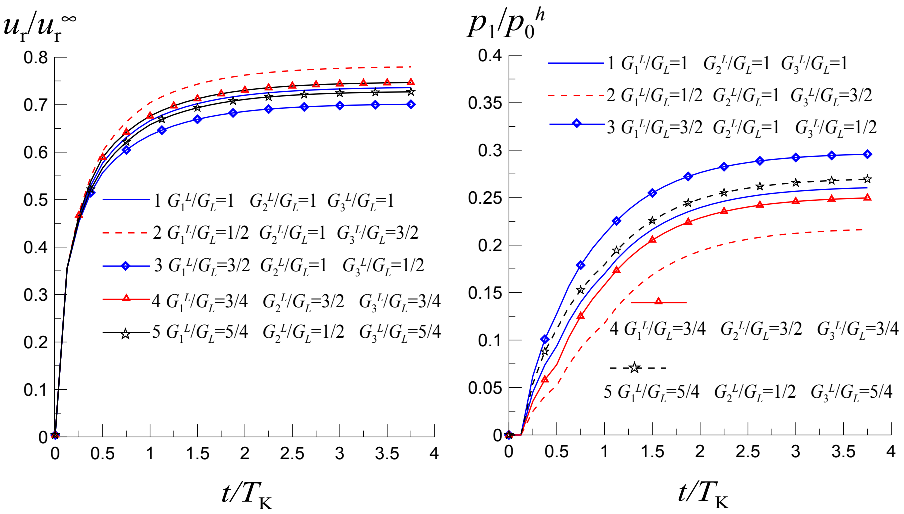

a) b)

Figure 14. Influence of liner shear modulus: a) normalized radial convergence versus normalized time; b) normalized support pressure versus normalized time for various relative modulus between liners (with same n_s=20).

Table 2 Material parameters of the liners.

Parameters	The first liner	The third liner
Young's Modulus	$E_1^L = 2.0\times10^4$ MPa	$E_3^L = 2.5\times10^4$ MPa
Poisson's Ratio	$\nu_1^L = 0.2$	$\nu_3^L = 0.2$
Thickness	$d_1 = 100$ mm	$d_3 = 300$ mm

The second liner

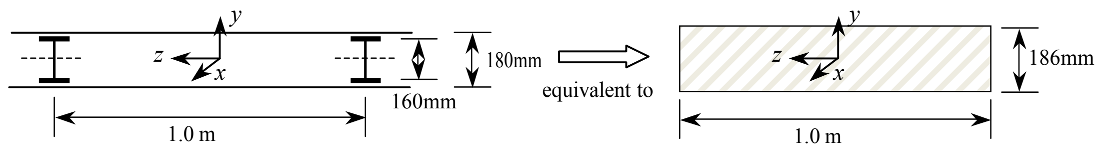

	Steel Set	Shotcrete	Equivalent section
Thickness	160mm	180mm	$d_2 = 186$ mm
Area of the section	2.6×10^{-3} m^2	——	——
Second moment of area of the section	1130×10^4 mm^4	——	——
Young's Modulus	2.0×10^5 MPa	2.0×10^4 MPa	2.29×10^4 MPa
Poisson's ratio	0.25	0.2	0.2

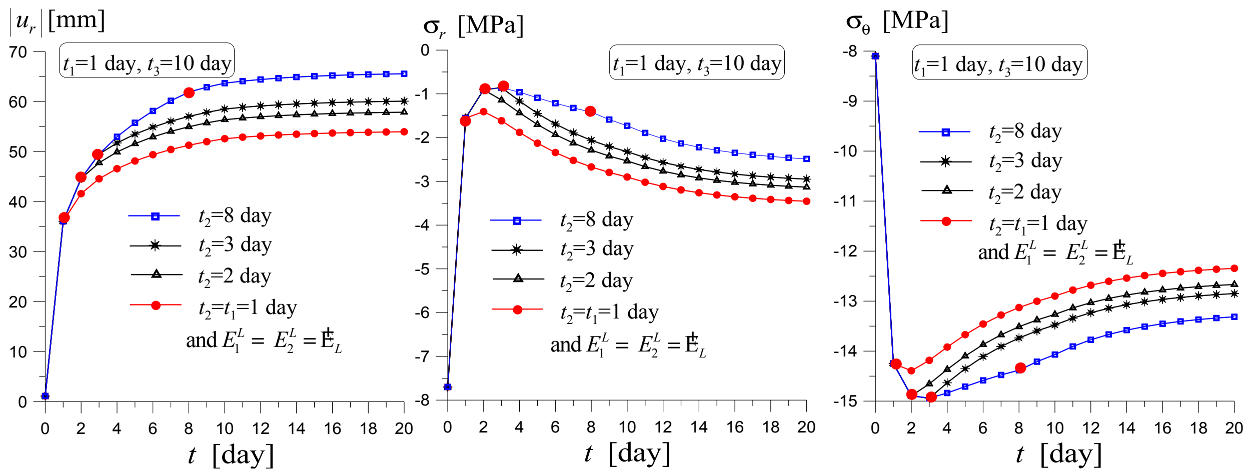

(a) (b) (c)

Figure 15. Displacements and stresses calculated at the interface between rock and the first liner (r=6.2m) versus time for various installation times of the second liner. Red circles (●) indicate the installation times of the second liner. a) radial convergence versus time; b) radial stress versus time; c) hoop stress versus time.